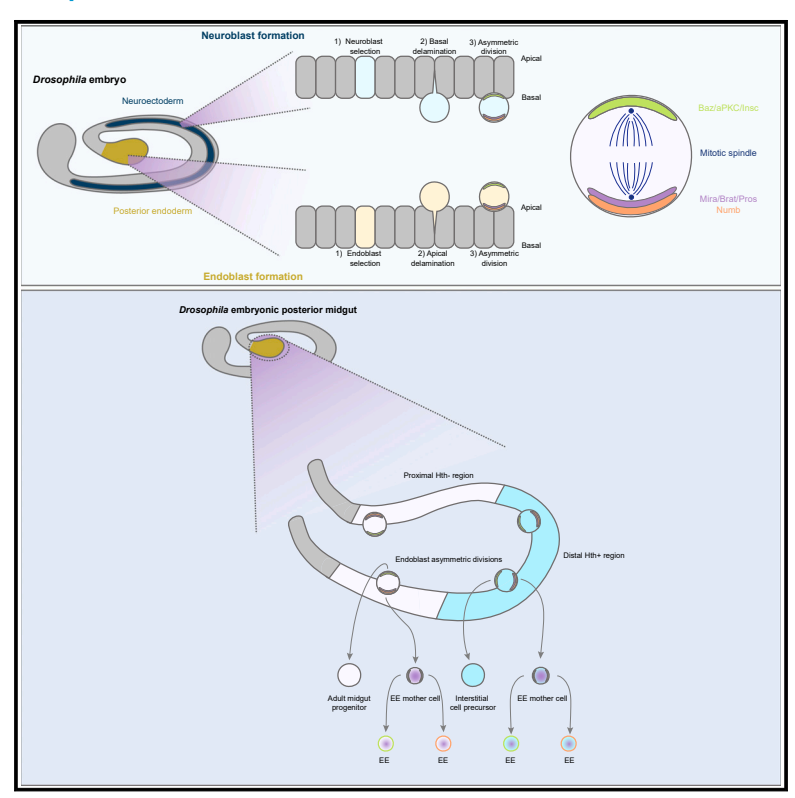
# The *Drosophila* adult midgut progenitor cells arise from asymmetric divisions of neuroblast-like cells

#### **Graphical abstract**



#### **Authors**

Andrew T. Plygawko, Camille Stephan-Otto Attolini, Ioanna Pitsidianaki, David P. Cook, Alistair C. Darby, Kyra Campbell

#### Correspondence

kyra.campbell@sheffield.ac.uk

#### In brief

Plygawko et al. show that the adult midgut progenitor cells, which give rise to all cells in the adult midgut, form from the asymmetric division of cells in the embryonic endoderm. These cells, which they call endoblasts, show many similarities with neuroblasts, the progenitor cells of the nervous system.

#### **Highlights**

- Endoblasts in the embryonic endoderm show many parallels with neuroblasts
- Endoblasts divide asymmetrically with larger cells forming either an AMP or ICP
- Smaller cells inherit Pros, Numb, and Brat to form an enteroendocrine mother cell
- Hth patterns endoblasts along the proximal-distal axis to specify AMP vs. ICP fate







#### **Article**

# The *Drosophila* adult midgut progenitor cells arise from asymmetric divisions of neuroblast-like cells

Andrew T. Plygawko,¹ Camille Stephan-Otto Attolini,² Ioanna Pitsidianaki,³ David P. Cook,⁴,⁵ Alistair C. Darby,⁶ and Kyra Campbell¹,⁻,\*

#### **SUMMARY**

The *Drosophila* adult midgut progenitor cells (AMPs) give rise to all cells in the adult midgut epithelium, including the intestinal stem cells (ISCs). While they share many characteristics with the ISCs, it remains unclear how they are generated in the early embryo. Here, we show that they arise from a population of endoderm cells, which exhibit multiple similarities with *Drosophila* neuroblasts. These cells, which we have termed endoblasts, are patterned by homothorax (Hth) and undergo asymmetric divisions using the same molecular machinery as neuroblasts. We also show that the conservation of this molecular machinery extends to the generation of the enteroendocrine lineages. Parallels have previously been drawn between the pupal ISCs and larval neuroblasts. Our results suggest that these commonalities exist from the earliest stages of specification of progenitor cells of the intestinal and nervous systems and may represent an ancestral pathway for multipotent progenitor cell specification.

#### INTRODUCTION

Stem cells are defined by their capacity to self-renew and to generate daughters that differentiate into one or more cell types. Since the identification of intestinal stem cells (ISCs) in the adult Drosophila midgut and the demonstration that they share similarity with their vertebrate counterparts, 2-4 ISCs have emerged as a valuable model for studying many aspects of stem cell biology, including stemness, niche maintenance, aging, and pathogenesis.<sup>5,6</sup> The ISCs are derived from a subpopulation of progenitor cells, the adult midgut progenitor cells (AMPs), during pupal stages. 7-9 The AMPs share many similarities with the ISCs, undergoing periods of self-amplification and being capable of differentiating into distinct intestinal cell types, namely the absorptive enterocytes (ECs) and secretory enteroendocrine cells (EEs). 10 While the origin and regulation of the ISCs in the pupal and adult midgut are well understood, precisely where and how the AMPs arise is less clear, raising the question of how such multipotent progenitor cells are formed in the embryo.

In *Drosophila*, the embryonic midgut originates from two groups of endodermal cells at either pole of the blastoderm. During gastrulation, these cells undergo an epithelial-to-mesenchymal transition (EMT), converting to unpolarized masses of

mesenchymal cells which migrate through the embryo. 11-14 Previous studies suggested that the AMPs and two other intestinal cell types, the EEs and interstitial cell precursors (ICPs), delaminate from the endodermal-epithelium before migration and that this is driven by proneural and neurogenic gene activity. 15 While initially the proneural and neurogenic genes are expressed throughout the endodermal-epithelium, Notch activity restricts proneural gene expression to a single cell through the process of lateral inhibition, leading to the regularly spaced segregation of cells throughout the tissue. 15 Showing parallels with the specification of epidermal precursors vs. neuroblasts in the neuroectoderm, 16 Notch activity in the majority of cells drives them to adopt an epithelial fate and form the larval ECs, the so-called principle midgut epithelial cells (PMECs),11 whereas cells that express proneural genes will delaminate from their neighbors and become either an AMP, ICP, or EE<sup>15,17</sup> (Figure 1A). Each of these cells take on different roles, with the AMPs acting as progenitor cells for the entire adult midgut, and the EEs and ICPs differentiating to perform distinct intestinal functions. It is currently unknown precisely when and how these three different subsets of intestinal cell types are determined downstream of proneural and neurogenic gene activity.

Here, we generated a single-cell transcriptomic atlas of posterior intestinal tract development that allowed us to follow the



<sup>&</sup>lt;sup>1</sup>School of Biosciences, The University of Sheffield, Sheffield S10 2TN, UK

<sup>&</sup>lt;sup>2</sup>Institute for Research in Biomedicine (IRB Barcelona), The Barcelona Institute of Science and Technology, Barcelona, Spain

<sup>&</sup>lt;sup>3</sup>Department of Cell and Developmental Biology, University College London, London WC1E 6DE, UK

<sup>&</sup>lt;sup>4</sup>Cancer Therapeutics Program, Ottawa Hospital Research Institute, Ottawa, ON, Canada

<sup>&</sup>lt;sup>5</sup>Department of Cellular and Molecular Medicine, University of Ottawa, Ottawa, ON, Canada

<sup>&</sup>lt;sup>6</sup>Institute of Infection, Veterinary and Ecological Sciences, University of Liverpool, Liverpool, UK

<sup>&</sup>lt;sup>7</sup>Lead contact

<sup>\*</sup>Correspondence: kyra.campbell@sheffield.ac.uk https://doi.org/10.1016/j.devcel.2024.10.011



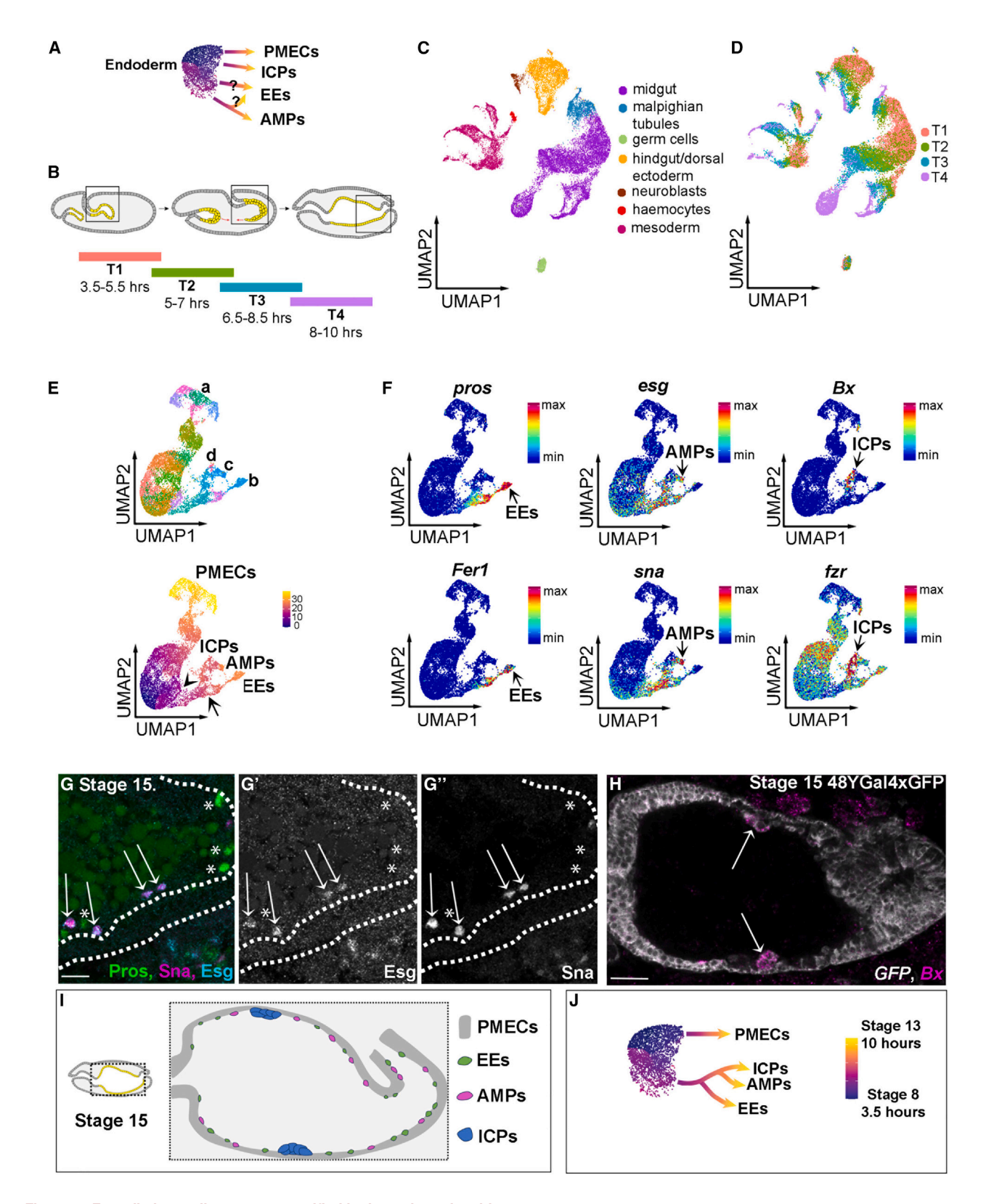


Figure 1. Four distinct cell types are specified in the embryonic midgut

(A) Schematic of the current understanding of midgut cell specification.

(B) Schematic of Drosophila embryos over 3.5–10 h of embryogenesis. Boxes show approximate depiction of regions dissected from living embryos.

(C) UMAP representation of batch-corrected scRNA-seq data colored for cell type based on marker gene expression.

#### **Article**



emergence of the different cell types in the posterior endoderm. These data suggested that AMPs, ICPs, and EEs do not delaminate directly from the outer layer of the early endoderm but instead arise from neuroblast-like cells, which we have termed endoblasts. We found that endoblasts apically delaminate from the outer epithelial layer of the endoderm, undergo an asymmetric cell division, and generate the three non-epithelial cell types found in the embryonic midgut. While one daughter cell will go on to generate cells of the EE lineage, the fate of the other daughter depends on its position within the endoderm, and patterning by homothorax (Hth). AMPs will form from the larger endoblast daughter in the more proximal regions, whereas the larger daughter cells from Hth+ endoblasts in the distal tip generate ICPs. We further show that the daughter cells that give rise to the EE population subsequently undergo a second asymmetric cell division to produce further diversity. This cascade of divisions parallels both the generation of ISCs and EEs in the pupal midgut and the formation of the embryonic and larval nervous systems.

#### **RESULTS**

## Single-cell transcriptomic atlas of the developing posterior intestinal tract and surrounding tissues

To follow the emergence of different cell types from the endoderm germ layer, we dissected the posterior intestinal tract and surrounding regions from living Drosophila embryos and carried out single-cell RNA sequencing (scRNA-seq) (Figure 1B). We staged embryos in 4 time windows, from prior to the generation of the distinct midgut cell types until the onset of the formation of the mature embryonic intestinal epithelium (Figure 1B: see STAR Methods and Broadie et al. 18). Interrogation of unsupervised cell clusters using markers for tissues in the posterior region of the embryo confirmed that the majority of cells in our dataset were from the posterior midgut (Figures 1C, S1A, and S1B). The dataset also included other cell types in the dissected regions, including cells of the Malpighian tubules, hindgut/dorsal ectoderm, neuroblasts, mesoderm, hemocytes, and germ cells (Figures 1C, S1A, and S1B). Given that cells appeared to be ordered temporally along the uniform manifold approximation and projection (UMAP) embedding (Figure 1D), we applied Monocle, an algorithm that computationally orders individual cells according to progress through a biological process, without prior knowledge of the genes that define this progress. 19 This leads to the ordering of cells along an inferred pseudotime. Gratifyingly, we found a good match between ordering the cells according to our collection windows vs. to pseudotime (Figure S1C). This gave us confidence to use the combined scRNA-seq datasets to investigate the earliest stages of cell specification within the endoderm.

## The posterior midgut primordium gives rise to four transcriptionally distinct cell clusters

We next isolated the posterior midgut population from our scRNA-seq dataset and performed unsupervised clustering and pseudotime prediction (see STAR Methods). As pseudotime can act as a measure of how differentiated a cell is, <sup>19</sup> these analyses indicate that from a pool of relatively undifferentiated cells, posterior midgut cells follow different trajectories toward four transcriptionally distinct endpoints (Figure 1E, endpoints are labeled a–d). These data are in line with previous genetic and histological studies, <sup>15,17</sup> which have shown that endoderm cells are specified into four populations of midgut cells by midembryogenesis.

The majority of posterior midgut cells follow the path toward a cell type that expresses genes characteristic of PMECs (**a** in Figure 1E), including the smooth septate junction components *Tetraspanin2a* (*Tsp2a*),<sup>20</sup> *mesh*,<sup>21</sup> *snakeskin* (*ssk*),<sup>21</sup> *hoka*,<sup>22</sup> and the GATA factor *grain* (*grn*)<sup>23</sup> (Figures S2A and S2B; Table S1). To understand which midgut cell types are represented by the terminal states **b**, **c**, and **d**, we identified gene expression patterns unique to each population.

Prospero (Pros) is highly expressed in cells at endpoint **b**. Pros has been a controversial midgut cell marker in the early embryo, with various reports suggesting it marks AMPs<sup>10,24–26</sup> and others suggesting that it marks emerging EEs.<sup>17,27</sup> We find that in addition to *pros*, cells at endpoint **b** express the transcription factors (TFs) 48 related 1 (Fer1), Hairy/E(spl)-related with YRPW motif (hey), and homeobrain (hbn) (Figures 1F and S2C; Table S1). As Pros is a key determinant of pupal and adult EE cell fate, and these three TFs have all recently been implicated in specifying subsets of EEs,<sup>27,28</sup> this suggests that cells in endpoint **b** are the cells that will form the EEs in the embryonic and larval midgut.

In contrast, cells at endpoint **c** do not express *pros* but instead show upregulation of the EMT-transcription factor (EMT-TF) escargot (esg), a known marker for AMPs and pupal ISCs. <sup>7,9,29</sup> We also found high expression of two other EMT-TFs, snail (sna) and zinc finger homeodomain 2 (zfh2), which is notable, as EMT-TFs have been implicated in promoting stemness in many contexts<sup>30</sup> (Figures 1F and S2D; Table S1). Another highly expressed gene in endpoint **c** cells is headcase (hdc) (Figure S2D), which is required for the survival of adult progenitor cells in the *Drosophila* tracheal system and imaginal discs to adulthood. <sup>31,32</sup> Together, this suggests that the cells at endpoint **c** are the AMPs. To investigate further, we examined Esg and

<sup>(</sup>D) Same as (C) but annotated for the dissection time window.

<sup>(</sup>E) UMAP of midgut cells colored by unsupervised cell state clustering (top) or pseudotime (bottom) (a-d denote four predicted end states). The arrowhead and arrow indicate branch points.

<sup>(</sup>F) UMAPs of marker genes expressed in distinct subtypes of midgut cells colored by gene expression level.

<sup>(</sup>G) Immunofluorescence for Pros (green), Esg (cyan), and Sna (magenta) in a stage-15 embryo. Arrows show AMPs, asterisks highlight EEs, and white dotted lines outline PMECs.

<sup>(</sup>H) FISH for Bx in stage-15 embryos, arrows point to ICPs. All midgut cells are probed for gfp mRNA driven using the midgut-expressing 48YGal4.

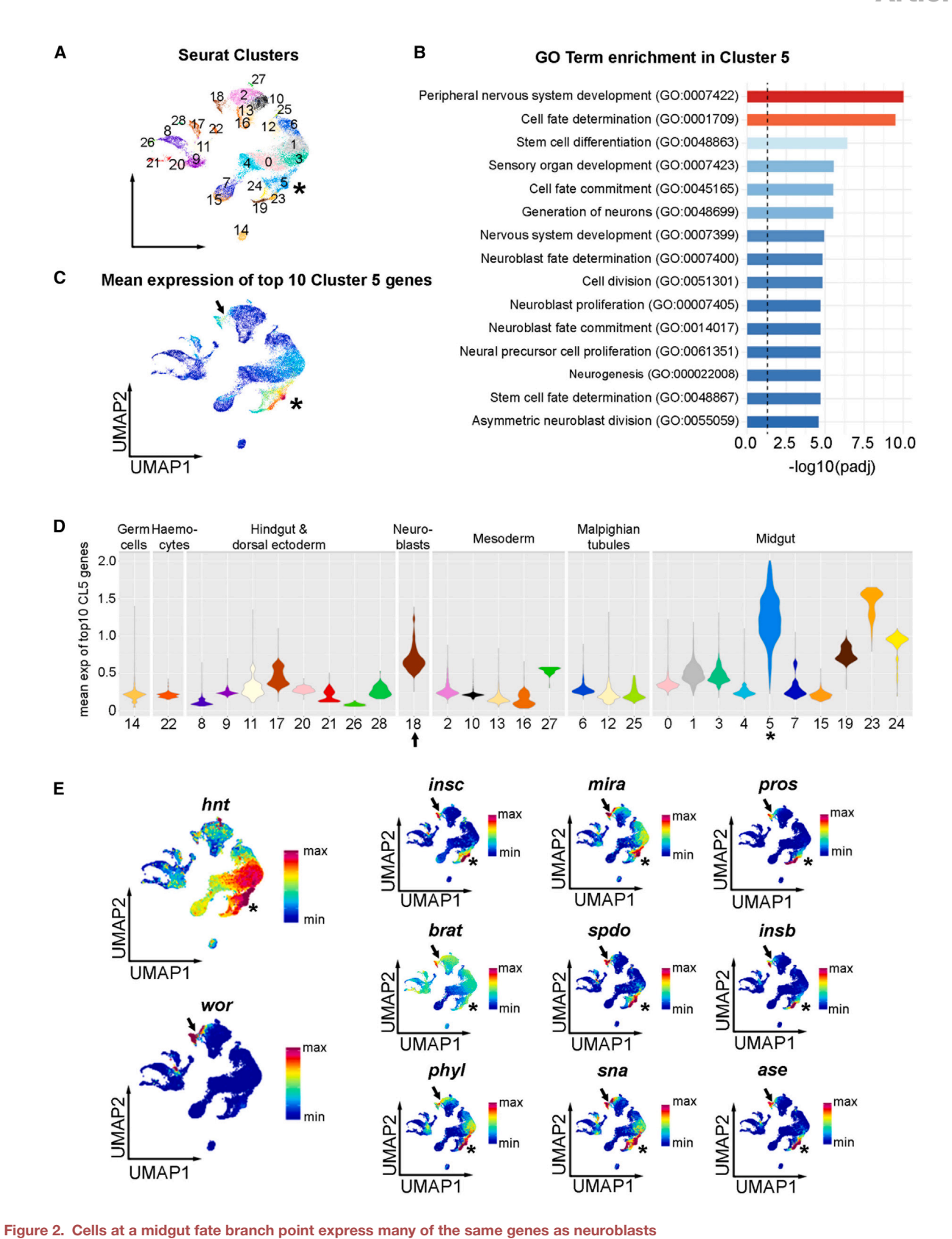
<sup>(</sup>I) Schematic diagram showing the localization of the distinct midgut cell types in a stage-15 embryo.

<sup>(</sup>J) Schematic of a revised model for midgut cell specification.

Scale bars, 10  $\mu m$  (G) and 25  $\mu m$  (H).

See also Figures S1 and S2 and Table S1.





(A) UMAP of scRNA-seq data colored by unsupervised cell state clustering, with clusters numbered. Cluster 5 is highlighted with an asterisk.

(B) Graphical representation of the overrepresented GO annotation classes from the top 50 genes expressed in cluster 5.

(legend continued on next page)

#### **Article**



Sna expression in the midgut of stage-15 embryos, which is well after midgut cell specification occurs and when the different cell types occupy distinct positions within the midgut. 14,17 Immuno-fluorescence (IF) staining for Esg and Sna, together with the EE marker Pros, revealed co-expression of Esg and Sna in small cells sitting on the inner surface of the midgut epithelium, the AMPs (Figure 1G, arrows). Pros also stains small cells sitting on the apical side of the PMECs (Figure 1G, asterisks), showing that in stage-15 midguts, the EEs and AMPs localize to the inner face of the PMECs and are interspersed with each other, as suggested previously 17 (Figures 1G and 1I).

While endpoint **d** is located on the same trajectory as AMPs, there are clear differences in gene expression between these two cell types. Cells at endpoint d do not express esg, sna, zfh2, or hdc, but show high expression of Beadex (Bx), a LIM domain only protein, and fizzy-related (fzr) (Figure 1F; Table S1). The increased expression of fzr is particularly interesting, as a key phenotypic difference between AMPs and ICPs is in their nuclear size, with ICP nuclear size already double that of AMP nuclei in stage-12 embryos (Figure S2F). While AMPs remain small and diploid throughout development, the nuclei of ICPs become even larger<sup>11,14,15,33</sup> and Fzr is a known regulator of endoreplication.34,35 We also find that expression of the Hox gene labial (lab) and defective proventriculus (dve) overlap with both cells in endpoint d, and a subset of PMECs (Figure S2E). These genes have previously been associated with the formation of the gastric region of the midgut, in which the polyploid interstitial cells sit. 36-39 Accordingly, FISH for Bx shows it localizes to cells with large nuclei localized at the junction of the anterior and posterior midgut—as previously described for the positioning of ICP cells mid-embryogenesis<sup>11</sup> (Figures 1H arrows and 1I).

## The AMPs, ICPs, and EEs form from a common intermediate cell population

Overall, the scRNA-seq data support previous work suggesting that midgut cells are specified into four distinct cell types in the embryo: PMECs, AMPs, ICPs, and EEs (Figures 1F-1I and S2; Tepass and Hartenstein<sup>15</sup> and Takashima et al.<sup>17</sup>). However, the branching points implied by pseudotime and the ordering of cells according to dissection times differ from what has been proposed previously based on genetic and morphological studies. Specifically, it has been suggested that AMPs, ICPs, and EEs delaminate directly from the epithelial endoderm, or even that EEs form from a subset of AMPs. 15,17 This scenario (Figure 1A) should lead to two or three branch points early on in the trajectory, but we find just one branch point at early time points (Figure 1E, bottom, arrowhead) and a second branch point later (Figure 1E, bottom, arrow). At this second branch point, one branch gives rise to EEs and the other to AMPs or ICPs (Figure 1E, bottom). This suggests that embryonic midgut cells are generated in a different manner than previously proposed (Figure 1J).

The existence of just one early branch point on the path to becoming AMPs, ICPs, and EEs suggests that these cells arise

from a common intermediate cell type. This appears on the UMAP as cluster 5, a cell cluster which encompasses cells around the branch point and lies on the trajectory to all cells that will form an AMP, ICP, and EE (Figure 2A, cluster 5, asterisk). To characterize this intermediate cell, we extracted the globally distinguishing genes for cluster 5 (Figure 2A, asterisk; Table S2) and carried out gene set enrichment analysis (Figure 2B). Overrepresented Gene Ontology (GO) terms included categories involved in stem cell differentiation and cell fate determination, as expected. However, we were surprised to find that the majority of other enriched GO terms related to nervous system development, sensory organ development, neuroblast fate determination/commitment, and asymmetric neuroblast division (Figure 2B). Furthermore, when we extracted the top 10 genes expressed in cluster 5 and examined the computed mean expression in all other cells in our dataset, we found that these genes are also highly expressed in neuroblasts (Figures 2C and 2D).

We next interrogated cluster 5 cells for the expression of genes known to regulate neuroblast asymmetric division and fate and found a large number expressed in both neuroblasts and this midgut-associated cluster 5 (Figure 2E, neuroblasts arrow, midgut cluster 5, asterisks), including genes involved in: the asymmetric division of neuroblasts-inscuteable (insc) and miranda (mira); cell fate determination—pros and brain tumor (brat); and negative regulation of the Notch pathway-sanpodo (spdo), insensible (insb), and phyllopod (phyl). The EMT-TF sna and the proneural gene asense (ase), both of which are drivers of multipotency, 40 are similarly expressed in cluster 5 (Figure 2E). We also noted expression patterns specific to each population (hnt and wor; Figure 2E), thereby precluding the possibility of artifacts associated with doublets in the dataset. Thus, our scRNA-seq data suggest that there is an intermediate midgut cell population that shows a highly overlapping gene expression with neuroblasts, the multipotent progenitors of the nervous system.

## Cells delaminate from the endoderm-epithelium and form a neuroblast-like progenitor cell

Embryonic neuroblasts undergo asymmetric divisions to give rise to two daughters of unequal size and distinct fates. The larger daughter cell retains multipotent neuroblast identity, while the smaller daughter cell is committed to differentiation. <sup>41</sup> Key features of neuroblast division are the asymmetric localization of cell fate determinants that form cortical crescents during mitosis and the orientation of the mitotic spindle orthogonal to the cortical protein crescents. Our finding that there is a neuroblast-like cell in the endoderm aligns with previous observations of crescents of Insc and Pros in cells within the early endoderm, <sup>25,26,42</sup> although this expression of Insc and Pros had been attributed to the AMPs. <sup>25,26,42</sup>

To investigate for the presence of neuroblast-like cells in the early endoderm, we stained stage-10 embryos for the neuroblast apical complex protein Bazooka (Baz), atypical protein kinase C (aPKC), the adaptor protein Mira, as well as the cell fate



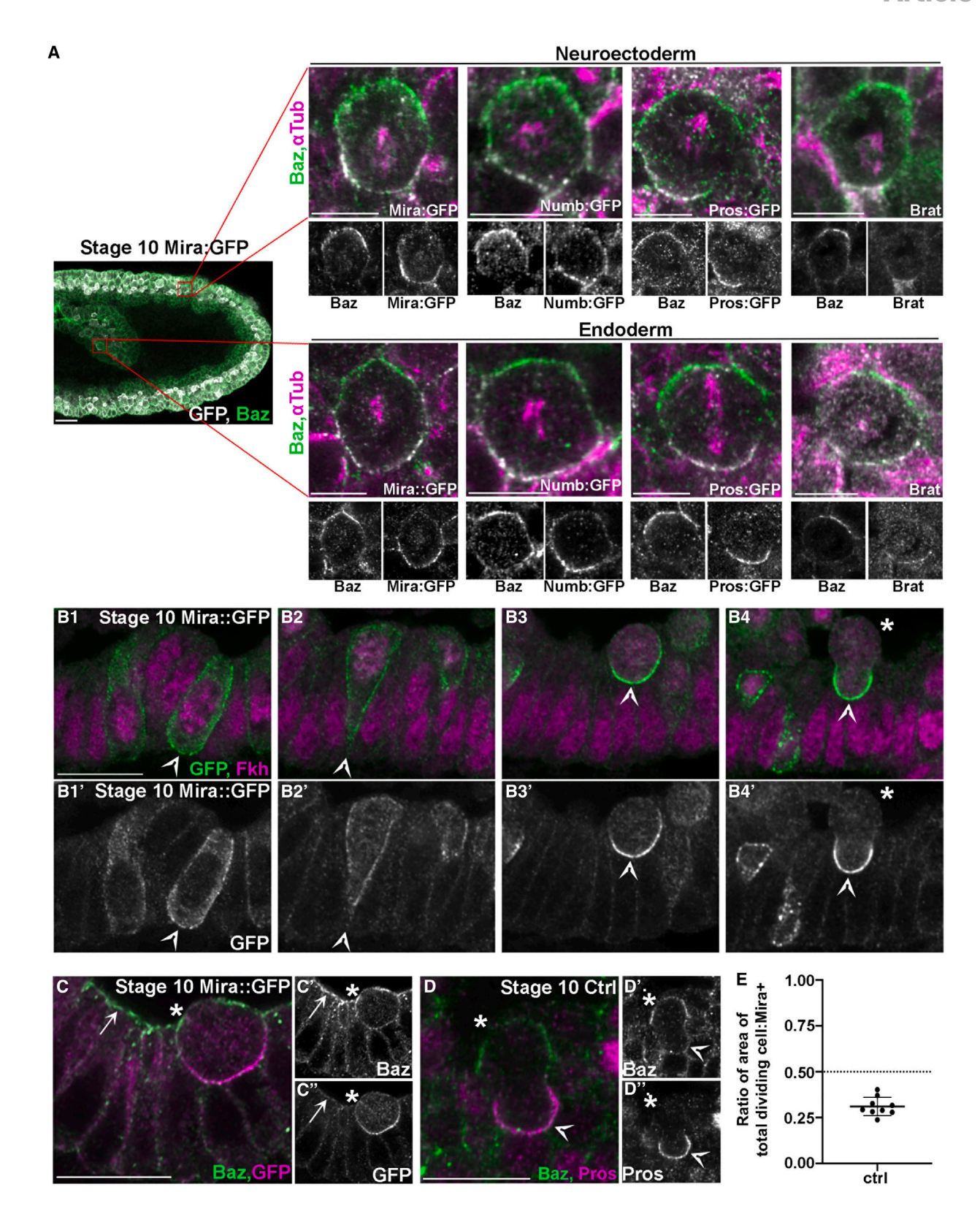


Figure 3. Neuroblast-like midgut cells undergo asymmetric cell divisions, giving rise to distinct midgut cell types

(A) Immunofluorescence of stage-10 embryos shows that dividing cells are present both in the neuroectoderm (right inserts, top) and endoderm (right inserts, bottom) and show polarized crescents of Baz, Mira, Numb, Pros, and Brat.

(legend continued on next page)

#### **Article**



determinants Numb, Pros, and Brat. As expected, we identified neuroblasts in the neuroectoderm that show Baz and aPKC in apical crescents, while Numb, Pros, and Brat localized basally together with their adaptor protein Mira (Figures 3A top row and S3). Strikingly, we also found cells of similar size and shape that showed identical protein localization delaminated from the endodermal-epithelium (Figures 3A bottom row and S3). Staining for  $\alpha$ Tubulin ( $\alpha$ Tub) revealed that, as in neuroblasts, mitotic spindles within these endoderm cells are oriented orthogonal to the cortical protein crescents (Figure 3A).

Expression of Mira in subsets of cells in the endoderm can first be detected while they are still part of the outer layer (Figure 3B1). These cells then become wedge shaped, constricting basally, and delaminate out of the apical side of the epithelium, (Figures 3B2 and 3B3), in the opposite manner to neuroblasts, which delaminate basally. As well as being a key regulator of apicobasal polarity in neuroblasts, Baz also regulates apicobasal polarity in epithelial cells. When staining for Baz together with Mira, we noticed that Baz is apically localized in the cells neighboring the delaminated Mira<sup>+</sup> cells, suggesting that the first cell delaminations initiate prior to EMT in the remaining epithelial cells, and therefore is a separable event (Figure 3C).

After the cells have delaminated, they divide to give rise to daughters of different sizes (Figures 3D and 3E), with the smaller cell lying close to the epithelium (Figures 3B and 3D arrowheads), and the larger cell facing the pocket (Figures 3B and 3D, asterisks). Mira segregates to the smaller daughter cells (Figures 3B, 4A, and 4B), together with Pros, Brat, and Numb. This suggests that the smaller daughter cell becomes an EE, similar to the neuroblast-derived ganglion mother cells (GMCs) that follow a differentiation path. Staining for Pros and markers for AMPs (Sna) and ICPs (Bx) suggests that the fate of the larger daughter cell that does not inherit Pros is regionally determined, with Pros negative cells in the proximal region of the posterior endoderm forming AMPs (Figures 4D and 4E) and cells in the distal tip forming ICPs (Figures 4D and 4E).

These data are further supported by the observation that despite *pros* expression being restricted to just endoblasts and EEs (Figures 4C, 4D, and 4F), when Pros-Gal4 is used to drive UAS-GFP, many of the inner layer of endoderm cells mosaically express GFP, not just the Pros<sup>+</sup> ones (Figures 4G and 4H). Costaining for GFP and cell-specific markers in Pros-Gal4>GFP embryos show clear GFP expression in a number of AMPs (Figure 4G) and ICPs (Figure 4H), as well EEs (Figure 4G). This suggests that GFP expression in AMPs and ICPs is due to the perdurance of GFP that they inherited from their mother cell—the asymmetrically dividing endoderm cell.

## Asymmetrically dividing endoderm cells use similar machinery to neuroblasts

These data show that parts of the molecular machinery that are deployed by neuroblasts to divide asymmetrically are also expressed in an endoderm-derived intermediate cell type and suggests that the unequal distribution of these molecules is leading to their asymmetric inheritance. To determine whether these molecules are functional, we examined mutants for mira or insc. In neuroblasts, mutation of mira or insc leads to a failure to form Pros crescents<sup>44,45</sup> or to mis-orientation of the mitotic spindle, 46 respectively. In line with what is seen in neuroblasts, 44 in mira mutants, Pros remains cytoplasmic in the intermediate cell throughout all stages of the cell cycle (Figures 5A, 5B arrows, and S4), while Baz is still able to form a crescent (Figures 5A, 5B, and S4). Likewise, in mutants for insc the mitotic spindle in intermediate cells no longer orientates orthogonal to the plane of the overlying epithelium, adopting a random angle within the cell (Figures 5C-5F) which affects the asymmetric segregation of cell fate determinants at metaphase (Figures S5A and S5B). Together, these results suggest that the intermediate cell type found within the endoderm uses similar machinery to neuroblasts to undergo asymmetric cell division. Given the similarities of this intermediate cell type with neuroblasts, and the fact that precursors of the nervous system and epidermis have been called neuroblasts and epidermoblasts, respectively, 16 we term these cells "endoblasts."

#### Endoblasts display "telophase rescue"

In *insc* mutants, the mitotic spindle orients at a random angle to the basal crescents of cell fate determinants, which should lead to some inheritance of Pros, Numb, and Brat by both daughter cells. To understand whether this leads to changes in midgut cell specification, we stained control and *insc* mutants for markers for AMPs (Sna), EEs (Pros), and ICPs (Bx). We counted the number of each cell type in the midguts of control and *insc* mutant stage-15 embryos (Figures 5G, 5H, and 5J) and found that rather than seeing a loss of one cell type, and increase in another, we see a general increase in EEs, AMPs, and ICPs in *insc* mutants, suggesting that specification of the different cell lineages does occur in *insc* mutants.

Since we expected changes in the inheritance of basal cell fate determinants by endoblast daughters to affect midgut cell fate decisions, we wondered if, in a further parallel with neuroblasts, the well documented telophase rescue phenomenon may be acting. Asymmetric divisions in neuroblasts requires both polarity proteins such as Baz, aPKC, and Par6 (the Par complex) and Lgl and Dlg to polarize the cortex, as well as a set of proteins including Insc, partner of inscuteable (Pins), and Gai proteins to orientate the spindle relative to cortex polarity. They act

See also Figure S3.

<sup>(</sup>B) Immunofluorescence for GFP (green) in embryos expressing endogenously tagged Mira, and Fkh (magenta) to visualize all endoderm nuclei. Apical is up, basal down. Arrowheads point to the basal side of delaminating endoblasts. Asterisks in B4 marks the larger Mira<sup>-</sup> daughter cell.

<sup>(</sup>C) Immunofluorescence staining for Baz (green) and GFP (magenta) in Mira::GFP embryos. The asterisk highlights an asymmetrically dividing endoblast, the arrow points to localized Baz in the surrounding midgut epithelium.

<sup>(</sup>D) Immunofluorescence for Baz (green) and Pros (magenta) in a stage-10 embryo shows an asymmetrically dividing endoblast; the side with Baz (asterisks) will give rise to the larger daughter.

<sup>(</sup>E) Quantification of the size difference between endoblast daughter cells. Each dot represents a dividing endoblast as shown in (D), the dotted line plots the expected value if both daughters were equal sizes. Solid line represents the mean, and error bars are standard deviation.

Scale bars, 25 μm (A, left) and 10 μm (all other images).



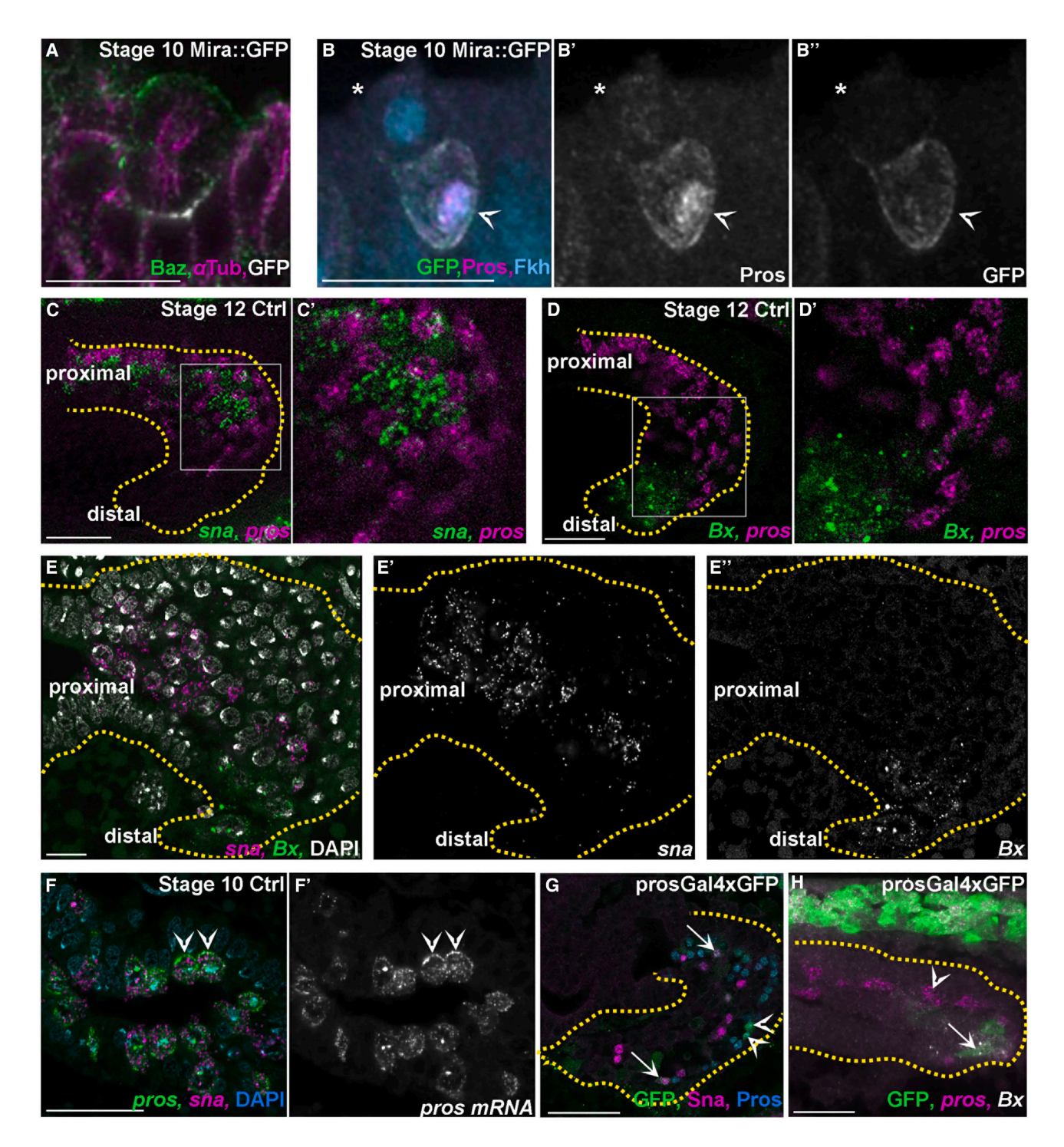


Figure 4. Endoblast daughters form the AMP, ICP, and EE populations

(A and B) Immunofluorescence for GFP (A, white, B, green), αTub (A, magenta), and Baz (A, green), Pros (B, magenta), or Fkh (B, cyan) in stage-10 embryos expressing endogenously GFP-tagged Mira. Asterisk marks the apical lumen, while the arrowhead indicates the newly formed Pros<sup>+</sup> nucleus of a presumptive EE cell. (C and D) FISH for sna (C, green) or Bx (D, green), and pros (magenta). White boxes are enlarged in (C') and (D').

(E) FISH for sna (magenta), Bx (green), and DAPI (white) in a stage-12 embryo.

(F) FISH for *pros* (green), *sna* (magenta), and DAPI (cyan) in a stage-10 embryo, arrowheads highlight apical crescents of *pros* RNA in dividing endoblasts. (G) UAS-GFP (green) driven with ProsGal4 expresses in both Pros<sup>+</sup> (cyan) and Snail<sup>+</sup> (magenta) cells, marking EEs (arrowheads) and AMPs (arrows), respectively. (H) UAS-GFP driven with ProsGal4 also marks *Bx*<sup>+</sup> (white) ICPs. Note that GFP<sup>+</sup>Bx<sup>+</sup> cells do not express *pros* mRNA (magenta). Yellow dotted lines outline the posterior midgut.

Scale bars, 25  $\mu m$  (E–H, left in C, and D) and 10  $\mu m$  (A and B).



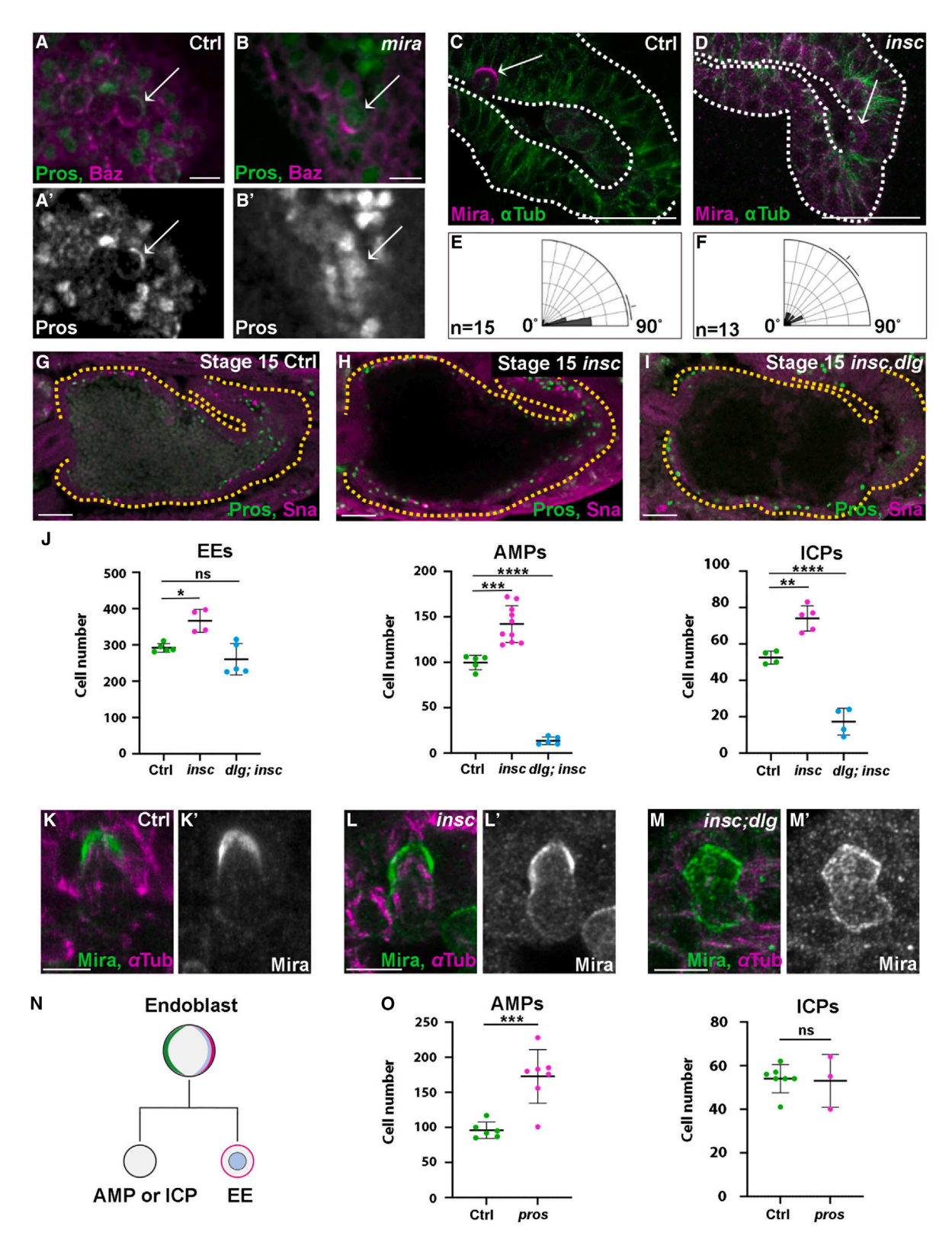


Figure 5. Telophase rescue ensures asymmetric inheritance of cell fate determinants for correct specification of AMP/ICP vs. EE cell fate (A and B) Immunofluorescence for Pros (green) and Baz (magenta) in stage-10 control (A) and mira mutant (B) embryos. Arrows highlight a dividing endoblast, pointing to the cortex opposite the Baz crescent.



through two partially redundant pathways: the Insc/Par complex pathway and the Insc-independent Dlg/Lgl, microtubule-dependent pathway.47 This was demonstrated in neuroblasts by following the cortical localization of Mira in wild-type and mutant neuroblasts at different stages of the cell cycle. 47 Wild-type neuroblasts show basal crescents for Mira at metaphase and telophase. 44,45 In contrast, insc mutant neuroblasts fail to localize Mira at metaphase but exhibit basal Mira localization at telophase—the so-called telophase rescue, 46 which is also seen in mutants for other components of this complex. 48,49 Similarly, dlg mutant neuroblasts also fail to form basal Mira crescents at metaphase, yet exhibit telophase rescue. 50 In contrast, insc; dlg double-mutant neuroblasts do not display telophase rescue of Mira localization, suggesting that this phenomenon is a result of either pathway directly or indirectly inducing basal cortical polarity in the absence of the other.<sup>47</sup>

To investigate whether telophase rescue also happens in endoblasts, we examined the localization of Mira in endoblasts at metaphase and telophase in wild-type, *insc* mutant, and *insc;dlg* mutant embryos. Staining for Mira in *insc* mutants shows that while endoblasts at metaphase fail to localize Mira properly (Figures 5D, S5A, and S5B), in telophase endoblasts, Mira is segregated to the smaller daughter cell as in controls (Figures 5K, 5L, S5C, and S5D). In *insc;dlg* embryos we found that the reorientation of Mira to align with the mitotic spindle of telophase endoblasts does not occur correctly, and consequently, Mira is distributed to both daughter cells (Figures 5M, S5C, and S5D). This suggested that in a further parallel to neuroblasts, *insc* and *dlg* act in a partially redundant manner in endoblasts to regulate the asymmetric segregation of cell fate determinants.

## The asymmetric division of endoblasts is required for normal midgut cell specification

To examine the role of asymmetric division of endoblasts in midgut cell specification, we next examined midgut cell specification in embryos mutant for both *insc* and *dlg*. Staining for markers for AMPs (Sna), EEs (Pros), and ICPs (Bx) in stage 15 *insc;dlg* mutant embryos suggests that while EEs are specified to near wild-type levels, both AMPs and ICPs are almost completely absent (Figures 5I and 5J). The fact that we find near normal levels of EEs in *insc*, *dlg* mutants suggests that when mis-specified the second daughter cell that would normally give rise to an AMP or ICP either dies or fails to turn on ter-

minal markers like Sna or Bx. These data suggest that in endoblasts, similar to that in neuroblasts, the correct inheritance of cell fate determinants by daughter cells and is crucial for the formation of both AMPs and ICPs. Taken together, our data support a model in which endoblasts divide asymmetrically to give rise to either an EE and an AMP, or an EE and ICP (Figure 5N).

In adult intestinal lineages, Pros is required for the correct specification of EE cells following ISC division<sup>51-53</sup> and drives EE exit from the cell cycle.<sup>54</sup> This parallels its role as a suppressor of stemness and proliferation in the Pros+ daughters of neuroblasts.55 Having shown that disrupting inheritance of cell fate determinants such as Pros led to a repression of AMP and ICP fate, we examined whether the disruption of Pros could result in ectopic AMP and ICP fate. We found a near-doubling in the number of AMPs in pros mutant embryonic midguts (Figure 50), suggesting that the endoblast daughters, which would otherwise become EEs, instead default to a progenitor cell fate. Given that Pros suppresses neuroblast fate genes in embryonic GMCs,<sup>55</sup> we hypothesized that a lack of Pros in the midgut may result in ectopic expression of endoblast fate genes in defective endoblast daughter cells. Accordingly, we found that Mira, which is normally only expressed in endoblasts during early asymmetric divisions, fails to be downregulated and remains expressed in a small number of cells in stage-15 midguts (Figure S6). In contrast, we do not see an increase in ICPs in pros mutants, suggesting that additional factors are required for cells to become ICPs.

Together, these results demonstrate that the asymmetric segregation of cell fate determinants results in the formation of the AMP, EE, and ICP lineages in the embryonic midgut. The aberrant inheritance of Pros, Brat, and Numb by the intended Baz<sup>+</sup> cell results in the collapse of the progenitor lineage, whereas the disruption of Pros function in the Mira<sup>+</sup> cell blocks their differentiation and exit from the cell cycle.

## Patterning by Hth determines the outcome of asymmetric endoblast divisions

We next sought to understand what determines whether the larger daughter cell of an endoblast will become an AMP or an ICP, which take on very different cell fates. The AMPs are multipotent cells, which will remain quiescent throughout embryogenesis, and then undergo several rounds of divisions to self-amplify in larval stages.<sup>7,9</sup> In contrast, ICPs will upregulate Fzr and undergo endoreplication,<sup>33</sup> a well reported function for Fzr.<sup>34,35</sup>

(C and D) Staining for microtubules ( $\alpha$ Tub, green) and Mira (magenta) in the stage-10 endoderm of control and *insc* mutant genotypes. Arrows point to dividing endoblasts. Dotted white lines outline the endodermal-epithelium.

(E and F) Rose plots for mitotic spindle orientation in control (E) and insc mutant (F) endoblasts. n is the number of endoblast spindles analyzed.

(G-I) Immunofluorescence for EEs (Pros, green) and AMPs (Sna, magenta) in stage-15 control (G), insc (H), and insc;dlg (I) embryos. Yellow dotted lines outline the midgut.

(J) Quantification of the numbers of EEs (Pros<sup>+</sup>), AMPs (Sna<sup>+</sup>), and ICPs (Bx<sup>+</sup>) in stage-15 control, *insc* mutant, and *insc; dlg* mutant embryos. Each data point is an individual embryo. Lines represent the mean, and error bars are standard deviation.

(K–M) (K) Immunofluorescence for Mira (green) and αTub (magenta) in control (K), insc (L), and insc;dlg (M) stage-10 embryos.

(N) Schematic of endoblasts dividing asymmetrically to give rise to an EE and either an AMP or ICP. The larger daughter cell that inherits apical proteins (green) become an AMP or ICP, while the smaller daughter which inherits Pros (magenta) becomes an EE.

(O) Quantification of the numbers of AMPs (Sna\*) and ICPs (Bx\*) in stage-15 control and pros mutant embryos. Each data point is an individual embryo. Lines represent the mean, and error bars are standard deviation.

Data analysis for (J) and (O): ordinary one-way ANOVA with Tukey post hoc test, \* $p \le 0.05$ , \*\* $p \le 0.01$ , \*\*\*\* $p \le 0.0001$ , \*\*\*\* $p \le 0.0001$ . Scale bars, 10  $\mu$ m (A and B), 25  $\mu$ m (C, D, and G–I), and 5  $\mu$ m (K–M).

See also Figures S4-S6.





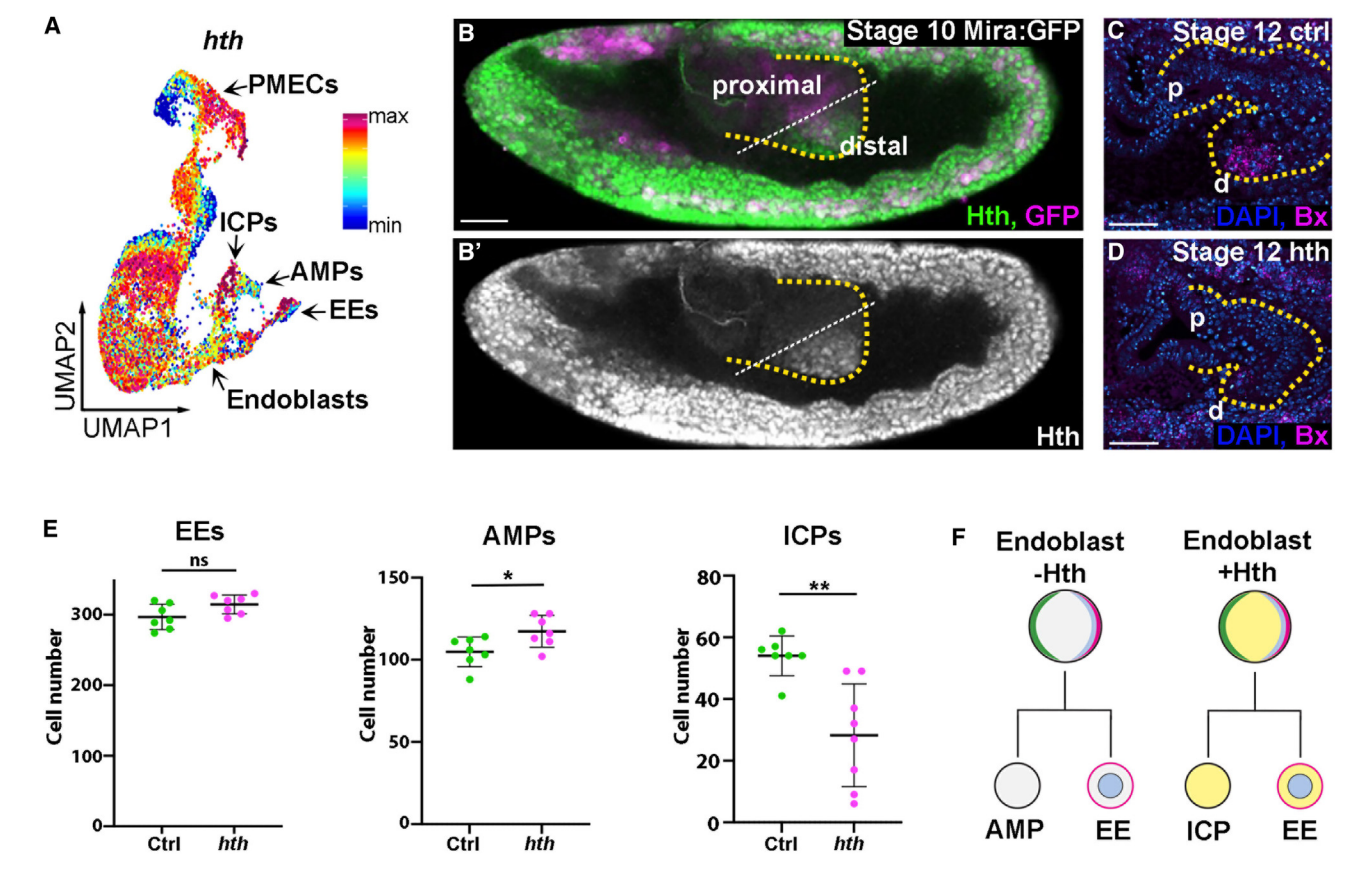


Figure 6. Hth is regionally expressed in the endoderm and determines AMP vs. ICP cell fate

(A) UMAP of midgut cells colored for hth expression.

(B) Immunofluorescence for Hth (green) and GFP (magenta) in a stage-10 embryo where endogenous Mira is tagged with GFP. White line demarks the proximal (left) and distal (right) region of the posterior midgut, which is outlined in yellow dashed lines.

(C and D) FISH for Bx in stage-12 control or hth mutant embryos.  $Bx^+$  cells at the front of the migrating endoderm in controls are ICPs. p, proximal; d, distal; yellow dashed lines outline the posterior midgut.

(E) Quantification of the number of EEs (Pros+), AMPs (Sna+), and ICPs (Bx+) in stage-15 (EEs, AMPs) or stage-12 (ICPs) embryos. Each data point is an individual embryo. Lines represent the mean, and error bars are standard deviation.

(F) Model for the role of Hth in patterning endoblasts. Endoblasts asymmetrically divide in both the Hth<sup>+</sup> (yellow cells) and Hth<sup>-</sup> (gray cells) regions of the endoderm. Daughters that inherit basal determinants (green) become AMPs if Hth<sup>-</sup> and ICPs if Hth<sup>+</sup>. Daughter cells that inherit Numb (magenta) and Pros (blue) become EEs in both regions.

Data analysis for (E): ordinary one-way ANOVA with Tukey post hoc test, \*p < 0.05, \*\*p < 0.005. Scale bars, 25 µm. See also Figure S7 and Table S3.

A comparison of gene expression between AMPs (cluster c) and ICPs (cluster d) (Table S3) showed that, while Bx and fzr are among the ICP-enriched genes, the gene most associated with ICPs is hth, a Pbc/Meis Hox cofactor. Interestingly, Hth and extradenticle (Exd) act together with Hox genes of the bithorax complex to pattern neuroblast identity in the abdomen, thereby determining the outcome of asymmetric neuroblast divisions. 56,57

Hth has previously been found expressed in the midgut during mid-embryogenesis, where it plays a role in the transduction of signaling from the underlying visceral mesoderm.<sup>58</sup> Our scRNA-seq data indicated expression of hth in the midgut from stages 8/9—well before interactions with the visceral mesoderm occur (Figure 6A). We confirmed this expression by immunostaining for Hth and FISH, which showed that in stage-10 embryos Hth is highly expressed in the distal tip of the endoderm (Figure 6B)—overlapping with ICPs and a subset of PMECs, EEs, and dividing endoblasts (Figure S7A-S7C). In contrast, Hth is not expressed in the proximal midgut, where AMPs are predominantly localized (Figures 6B and S7C). To investigate whether Hth is required for endoblasts to form ICPs, we examined hth mutants<sup>59</sup> for expression of the ICP marker Bx by FISH and found a significantly reduced number of ICPs (Figures 6C-6E). Additionally, in later-stage hth mutants, we observed only very few cells in the central region of the midgut with the large nuclei characteristic for ICPs (Figures S7D and S7E). Remarkably, while the numbers of ICPs are reduced, the numbers of AMPs increase in almost equal proportions, while there are no changes in the corresponding number of EEs (Figure 6E). These results suggest that it is the patterning of the endoderm downstream of Hth, and likely Hox gene regionalization, which determines whether an endoblast division will give rise to an EE and an AMP, or an EE and an ICP (Figure 6F).



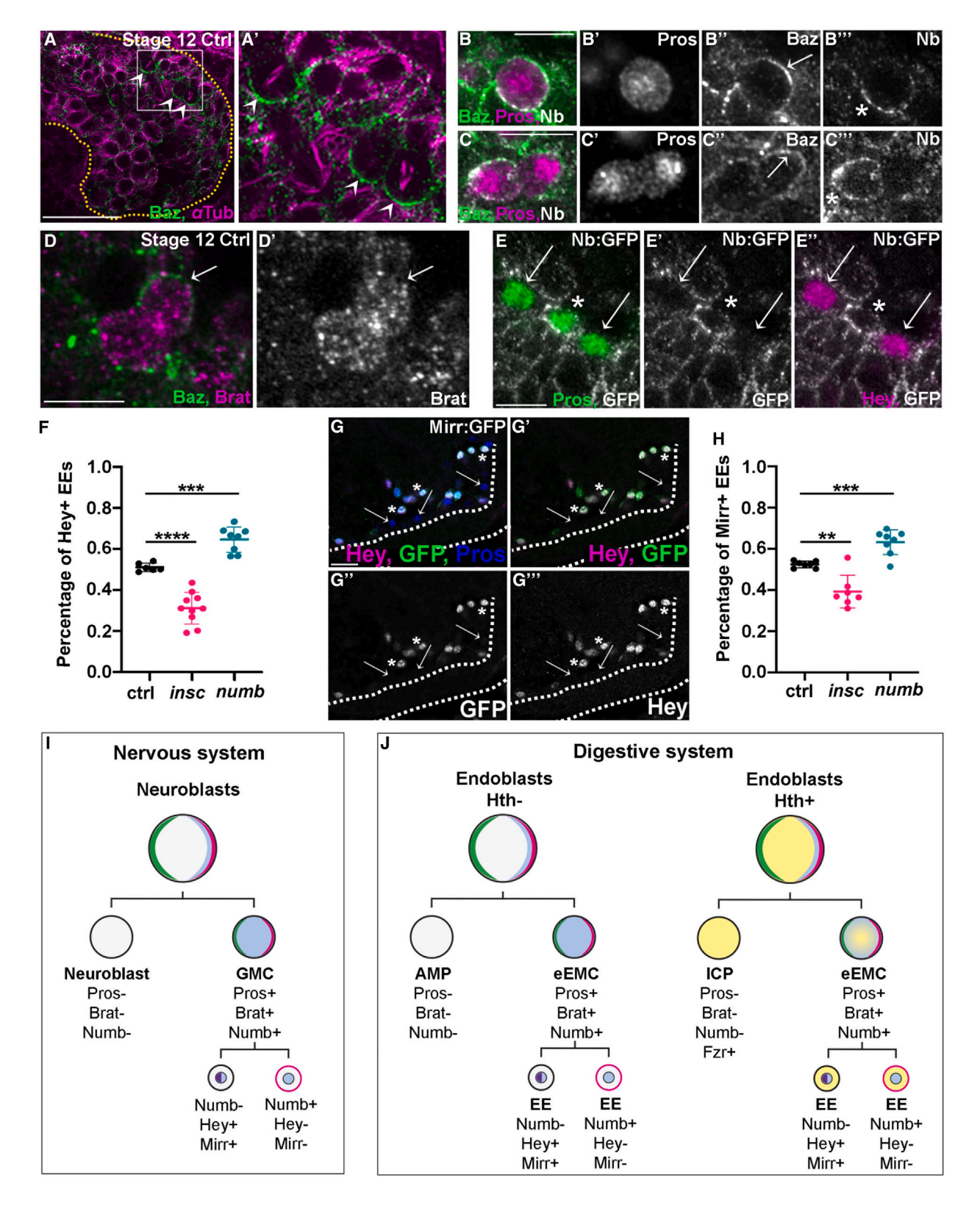


Figure 7. EEs undergo a second asymmetric division leading to differential Notch activation in daughter cells and specification of subpopulations of EEs

(A) Immunofluorescence for Baz (green) and αTub (magenta) in a stage-12 embryo. Arrowheads point to asymmetrically dividing cells. White box is enlarged in (A').

#### **Article**



## The Pros<sup>+</sup> endoblast daughter cell undergoes a second asymmetric division, generating distinct EE lineages

Our data show that in the Drosophila embryo common molecular mechanisms drive asymmetric divisions of intestinal and neural stem cells to generate multipotent progenitor cells. To determine whether there are additional similarities in how downstream cell lineages are determined, we focused on the Pros<sup>+</sup> daughter cell. In the embryonic nervous system, this cell is called the GMC and divides a second time. 41 The majority of GMC divisions are asymmetric. The fate of the two daughters is dictated by levels of Notch signaling, which is determined by differential inheritance of Numb, an inhibitor of Notch signaling. 60 Intriguingly, it has recently been proposed that there may be an asymmetric division of a Pros<sup>+</sup> midgut cell around embryonic stage 12-13,<sup>27</sup> and the number of Pros+ EEs has been reported to double mid-embryogenesis. 17 Notch-dependent Hey expression is detected in half of these,<sup>27</sup> mirroring the asymmetric expression of Hey after GMC divisions. 60 By immunostaining for Pros and αTub, we found that the Pros<sup>+</sup> midgut cells undergo a second asymmetric division, localizing Baz and Numb to opposing crescents (Figures 7A-7D). As a result, while all daughter cells inherit Pros and Brat (Figures 7C and 7D), one daughter inherits Numb, which represses Notch signaling (Figure 7E), whereas the other activates Notch, as seen by expression of the Notch target Hey (Figure 7E).

These findings suggested that the Pros<sup>+</sup> daughter of an endoblast division undergoes a second division, drawing parallels with GMCs and as well as the so-called enteroendocrine mother cells (EMCs) that have been described in the pupal midgut.<sup>29,61</sup> We therefore named this cell the embryonic EMC (eEMC). Insc is required for the correct orientation of GMC division with respect to the basal orientation of Numb. Accordingly, GMC daughter cells adopt equivalent cell fates in insc mutant embryos. 62 To determine whether the asymmetric division of EMCs plays a functional role in the establishment of unequal daughter EE cell fate, we stained for Hey in insc mutants and found that the proportion of Hey<sup>+</sup> EEs decreases significantly (Figure 7F). Furthermore, Numb is also required for the specification of EEs into distinct populations, as the Hey<sup>+</sup> EE population was significantly increased in mutants with reduced numb activity (Figure 7F). This suggests that Numb acts as a cell fate determinant in the embryonic midgut to produce EE diversity.

Beyond their similarities to nervous system development, the division of EMCs to produce distinct EE subtypes draws parallels with both the pupal and adult *Drosophila* midgut. In the pupal

midgut, an EMC is derived from the asymmetric division of a pupal ISC. This pupal EMC also divides asymmetrically with respect to Notch,29 although this appears independent of Numb activity, 61 and a role for Insc has not yet been described. Similarly, adult ISCs can divide to produce an EE progenitor cell, which divides again to produce EEs expressing different hormones.<sup>54</sup> The hormone signature of adult EEs is determined first by differential Notch activation, wherein Notch-inactive (class I) EEs express allatostatin C and Notch-active (class II) EEs express Tachykinin, 63 with further subtypes determined by regionalization along the midgut. The TF Mirror (Mirr) is expressed in class II EEs in the adult midgut in a Notch-dependent manner and is required for the expression of class II hormones. 28,64 To further establish the functional relevance of the eEMC asymmetric division in EE diversity, we assayed our scRNA-seq data for mirr expression and found that it expressed in the same subpopulation of EEs as hey.

To confirm this, we examined Mirr expression in the stage-15 midgut. First, we found that Mirr was expressed in approximately half of the EEs, consistent with its activation in only one of two eEMC daughters (Figures 7G and 7H). Next, we saw that Mirr and Hey were co-expressed in these EEs, consistent with their joint activation through Notch activity (Figure 7G). Finally, the number of Mirr<sup>+</sup> EEs also decreased significantly in *insc* mutants and increased in *numb* mutants (Figure 7H). This suggests that the specification of embryonic EE subpopulations is reminiscent of both the GMCs of the embryonic nervous system and the EE precursors of the adult midgut. Furthermore, it suggests that the Mirr<sup>+</sup>, Hey<sup>+</sup>, and Numb<sup>-</sup> cells will go on to form the Tk<sup>+</sup> EEs of the larval midgut, whereas the Mirr<sup>-</sup>, Hey<sup>-</sup>, and Numb<sup>+</sup> cells will form the presumptive AstC<sup>+</sup> class I EEs.

#### DISCUSSION

In most organisms the most fundamental type of stem or progenitor cell in our body, the primordial germ cell, is set aside early during embryogenesis and requires suppression of the somatic program. <sup>65</sup> In contrast, multipotent progenitor cells are generated from somatic tissue during later stages of development, after some degree of patterning and differentiation has already occurred. One of the most well-understood examples is *Drosophila* neuroblasts, which delaminate from the neuroectoderm and give rise to the entire nervous system of an animal. Previous work has shown that the neurogenic and proneural gene cassettes that act upstream of neuroblast specification in the

(B and C) Immunofluorescence for Baz (green), Pros (magenta), and GFP (white) in stage-12 embryos expressing GFP-tagged Numb. Pros<sup>+</sup> midgut cells undergo a second asymmetric division where Pros remains cytoplasmic (B and C, magenta), and Baz (B and C, green, arrow) and Numb (B and C, white, asterisks) localize to polarized crescents (B) and are differentially inherited (C).

<sup>(</sup>D) Immunofluorescence for GFP (magenta) and Baz (green) in GFP-tagged Brat-expressing embryos during the second asymmetric division.

<sup>(</sup>E) Immunofluorescence for GFP (white), Pros (green), and Hey (magenta) in stage-12 embryos expressing GFP-tagged Numb. Pros<sup>+</sup> EEs either express the Notch inhibitor Numb (E', white, asterisks) or the Notch target Hey (E'', magenta, arrows) at this stage.

<sup>(</sup>F) Quantification of the number of Hey<sup>+</sup> EEs in stage-15 ctrl, insc, and numb mutant embryos.

<sup>(</sup>G) Immunofluorescence for Hey (magenta), GFP (green), and Pros (blue) in stage-15 embryos expressing GFP-tagged Mirr. Arrows point to Pros<sup>+</sup>Hey<sup>-</sup>Mirr<sup>-</sup> cells, and asterisks highlight Pros<sup>+</sup>Hey<sup>+</sup>Mirr<sup>+</sup> cells.

<sup>(</sup>H) Quantification of the number of Mirr<sup>+</sup> EEs in stage-15 ctrl, *insc*, and *numb* mutant embryos.

<sup>(</sup>I and J) Diagram depicting the parallels between generation of the diverse cell types in the *Drosophila* nervous system (I) and digestive system (J). Yellow dotted lines in (A) outline the posterior midgut.

In (F) and (H), each data point is an individual embryo. Lines represent the mean, and error bars are standard deviation. \*\*p < 0.01, \*\*\*p < 0.001, \*\*\*\*p < 0.001, ordinary one-way ANOVA with Tukey post hoc test. Scale bars, 25  $\mu$ m (A), 5  $\mu$ m (B–E), and 10  $\mu$ m (G).



neuroectoderm are also active in the endoderm and required for midgut cell specification in the early embryo. 15 Here, we focus on events after Notch/Delta signaling has refined the expression of proneural genes to individual cells and show that there are many commonalities in how the progenitors cells of the nervous and intestinal system are generated, as well as in the initial stages of lineage specification (Figures 7I and 7J).

We show that three of the embryonic midgut cell types, the AMPs, ICPs, and EEs, are generated from a cell that delaminates from the endoderm-epithelium. These precursor cells-which we call endoblasts - show marked parallels with embryonic neuroblasts. First, after delamination, both cells undergo an asymmetric cell division to generate daughter cells of uneven size, with the smaller GMC/eEMC subsequently undergoing a second asymmetric division. Second, they both use Insc to orientate the mitotic spindle such that cortical Mira, Pros, Brat, and Numb are segregated to the smaller daughter to direct the cell toward differentiation. Third, when the spindle orientation is perturbed, loss of basal protein targeting at metaphase is rescued through telophase rescue.<sup>50</sup> Finally, the outcome of divisions of both cell types is determined by regional patterning, with Hth determining whether the larger daughter of an endoblast will produce an AMP or an ICP, with AMPs entering quiescence and remaining capable of renewed division at a later stage, and the Hth+ ICPs permanently exiting the cell cycle. Interestingly, in a subset of neuroblasts, Hth has been shown to trigger cell-cycle exit, although these cells then undergo apoptosis, rather than endoreplication.56

In addition to the marked similarities in how the progenitor cells of the nervous and intestinal systems are generated, there are also several differences. While neuroblasts delaminate basally from the neuroepithelium, the endoblasts delaminate apically. By delaminating basally, neuroblasts and their lineages can proliferate toward the center of the embryo, forming an internal central nervous system, which is further structured and stratified through orientation of the dividing stem cells. 66 However. were endoblasts to delaminate basally from the endoderm, this would perturb the endoderm-mesoderm contact required for embryonic midgut morphogenesis. 11,67 This may have placed constraints on the direction of delamination of endoderm cells and raises the question of how the mechanisms of delamination differ. Neuroblast delamination is driven through apical constriction and adherens junction disassembly, 68 whereas endoblasts undergoing delamination appear to maintain an apical surface and are basally constricted (Figures 3B2 and 3C). It would be interesting to examine whether the delamination of endoblasts is mechanistically similar to the apical extrusion of cells during epithelial homeostasis, where neighboring cells act to squeeze the extruded cells at their basal sides to remove them. 69,70

Another difference is that in the embryo neuroblasts divide multiple times, self-renewing with each asymmetric division, whereas the AMPs appear to immediately enter quiescence until early larval stages. 7-9 At this point, signals from the visceral muscle, which ensheathes the midgut, activates EGFR signaling in the AMPs and triggers their self-amplification through multiple rounds of symmetric divisions. While the majority of neuroblasts divide and then enter apoptosis once the neuronal lineages are complete, a subset of neuroblasts in the cephalic and thoracic regions enter quiescence later in embryogenesis before re-

entering mitosis in larval stages. 43 It will be interesting to see whether quiescence in AMPs and in these neuroblasts are driven through similar mechanisms.

During late metamorphosis, the majority of AMPs will activate Notch and differentiate into ECs, the absorptive epithelial cells that will line the majority of the adult midgut. A small fraction of AMPs maintain expression of esg, move basally, and form the pupal ISCs. These cells undergo a phase of self-amplification through symmetric divisions until the secretion of ecdysone from the dorsal internal oblique muscles triggers them to switch to asymmetric divisions.<sup>71</sup> Previous studies have highlighted the similarities between asymmetric divisions in pupal ISCs and embryonic and larval neuroblasts including the use of Baz/Par3 to define apical-basal polarity, the segregation of Mira and Pros to the basal daughter cell, and the generation of pupal EMCs, which divide once more using asymmetric Notch signaling to establish different faces among their daughters.<sup>29,61</sup> It is intriguing to note that all these features appear to be shared with the endoblast in the early embryo, suggesting that as for the nervous system, these mechanisms are reiterated throughout the different developmental stages.

Our study establishes that during Drosophila embryogenesis neural and ISC lineages arise through parallel cascades of asymmetric cell division driven by common molecular mechanisms. Drosophila neuroblasts have long been considered a powerful model for vertebrate neural stem cell biology, 72 and our results suggest that findings in this system may be more widely applicable than previously anticipated. Finally, they lend weight to the concept of a shared evolutionary origin for the digestive and nervous systems. This has largely been driven by studies in basal animals such as the cnidarian Nematostella vectensis. a useful model for the emergence of the early nervous system, and sea sponges. Despite not having a nervous system, a "neuroid" cell type was recently identified in the sea sponge Spongilla lacustris. Associated with the digestive chambers, it signals to digestive cells using gene networks shared with the neuronal synapses of higher organisms.<sup>73</sup> Additionally, while the nervous system and digestive system are derived from distinct germ layers in bilaterians-namely the ectoderm and endoderm, respectively-in Nematostella, there appears to be an overlap between these two germ layers,74 suggesting that while separated in bilaterians, the digestive system and nervous system may share a common ancestral tissue. Additionally, recent studies of Nematostella development showed that neurons and secretory cells originate from a common pool of progenitor cells, 75,76 potentially providing the first glimpse of a digestivenervous system intermediate cell type. Incorporating our findings in Drosophila, we propose that the putative ancestor tissue to the digestive and nervous systems possessed the ability to divide asymmetrically through the segregation of conserved cell fate determinants. This machinery, and the cell fate specialization it can provide, would then have been inherited by both organs to drive the functional specification of their constituent cell types.

#### **Limitations of the study**

A central finding in this paper was that the AMP, ICP, and EE cells in the embryonic midgut are derived from an intermediate cell type. While these findings were supported by scRNA-seq

#### **Article**



data, IF staining and FISH for cell markers in precisely staged fixed wild-type embryos, as well as cell counts in mutants, we have not yet followed the emergence of these cell types using live imaging. Imaging of the midgut at this stage of development is extremely challenging due to the timing of endoblast delamination and the depth of the tissue within the embryo. Development of live imaging should inform further on the temporal dynamics of this process. Furthermore, while other studies have focused on midgut cell behavior and fate during the larval-to-pupal and pupal-to-adult transitions, the precise behavior of midgut cells during late embryogenesis and early larval stages remains unclear. A full lineage tracing from embryo to adult using new markers provided in this study would be the definitive way of revealing the link between the endodermal cells in the embryo and the cells of the adult intestine and could also be refined to reveal deeper layers of regionalization that are likely formed during the earliest stages of embryogenesis.

#### **RESOURCE AVAILABILITY**

#### Lead contact

Further information and requests for resources and reagents should be directed to and will be fulfilled by the lead contact, Kyra Campbell (kyra.campbell@sheffield.ac.uk).

#### **Materials availability**

This study did not generate new unique reagents.

#### **Data and code availability**

- scRNA-seq data have been deposited at Biostudies and are publicly available as of the date of publication under accession number E-MTAB-13247. Accession numbers are listed in the key resources table. Microscopy data reported in this paper will be shared by the lead contact upon request.
- This paper does not report original code.
- Any additional information required to reanalyze the data reported in this paper is available from the lead contact upon reasonable request.

#### **ACKNOWLEDGMENTS**

We are thankful to the rest of the Campbell, Casali, Bulgakova, and Strutt labs for helpful discussions. We thank Christine Kocks, Nikolaus Rajewsky, and Robert Zinzen for their advice and sharing of protocols. We thank J. Casanova, B. Denholm, C. Desplan, M. Furuse, J. Januschke, M. Monastirioti, M. Weng, A. Wodarz, the Bloomington Stock Centre, and the Developmental Studies Hybridoma Bank for kindly sending us reagents. We thank David Strutt, Marysia Placzek, and Natalia Bulgakova for critical reading of the manuscript. scRNAseq library generation and sequencing were carried out by the Centre for Genomic Research, which is based at the University of Liverpool. This work was supported by a Wellcome Trust/Royal Society Sir Henry Dale Fellowship (grant number 204615/Z/16/Z). Editing help was provided by Life Science Editors.

#### **AUTHOR CONTRIBUTIONS**

This project was conceived by A.T.P. and K.C. The experimental design for the generation for the single cell atlas of posterior intestinal tract development was conceptualized by A.C.D. and K.C. and performed by I.P. and K.C. C.S.-O.A. carried out the scRNA-seq data processing and analysis, with D.P.C. giving additional bioinformatics support. A.T.P. designed, performed, and analyzed the biological experiments. A.T.P., C.S.-O.A., and K.C. wrote the manuscript, which was edited and reviewed by all authors.

#### **DECLARATION OF INTERESTS**

The authors declare no competing interests.

#### **STAR**\*METHODS

Detailed methods are provided in the online version of this paper and include the following:

- KEY RESOURCES TABLE
- EXPERIMENTAL MODEL AND STUDY PARTICIPANT DETAILS
  - o Fly Husbandry
  - Fly strains
- METHOD DETAILS
  - o Drosophila embryo fixation and immunofluorescence
  - o HCR in situ hybridisation
  - o Image collection
  - ScRNAseq methods
  - o ScRNAseq data processing
- QUANTIFICATION AND STATISTICAL ANALYSIS
  - Cell counting
  - o Spindle orientation
  - O Nuclear area and cell size measurement
  - Neuroblast and endoblast polarity quantification

#### SUPPLEMENTAL INFORMATION

Supplemental information can be found online at https://doi.org/10.1016/j. devcel.2024.10.011.

Received: February 28, 2024 Revised: July 21, 2024 Accepted: October 18, 2024 Published: November 11, 2024

#### **REFERENCES**

- 1. Molofsky, A.V., Pardal, R., and Morrison, S.J. (2004). Diverse mechanisms regulate stem cell self-renewal. Curr. Opin. Cell Biol. 16, 700-707. https:// doi.org/10.1016/j.ceb.2004.09.004.
- 2. Radtke, F., and Clevers, H. (2005). Self-renewal and cancer of the gut: two sides of a coin. Science 307, 1904-1909. https://doi.org/10.1126/science.
- 3. Ohlstein, B., and Spradling, A. (2006). The adult Drosophila posterior midgut is maintained by pluripotent stem cells. Nature 439, 470-474. https://doi.org/10.1038/nature04333.
- 4. Micchelli, C.A., and Perrimon, N. (2006). Evidence that stem cells reside in the adult Drosophila midgut epithelium. Nature 439, 475-479. https://doi. org/10.1038/nature04371.
- 5. Boumard, B., and Bardin, A.J. (2021). An amuse-bouche of stem cell regulation: underlying principles and mechanisms from adult Drosophila intestinal stem cells. Curr. Opin. Cell Biol. 73, 58-68. https://doi.org/10.1016/j.
- 6. Li, H., and Jasper, H. (2016). Gastrointestinal stem cells in health and disease: from flies to humans. Dis. Model. Mech. 9, 487-499. https://doi.org/ 10.1242/dmm.024232.
- 7. Jiang, H., and Edgar, B.A. (2009). EGFR signaling regulates the proliferation of Drosophila adult midgut progenitors. Development 136, 483-493. https://doi.org/10.1242/dev.026955.
- 8. Mathur, D., Bost, A., Driver, I., and Ohlstein, B. (2010). A transient niche regulates the specification of Drosophila intestinal stem cells. Science 327, 210-213. https://doi.org/10.1126/science.1181958
- 9. Micchelli, C.A., Sudmeier, L., Perrimon, N., Tang, S., and Beehler-Evans, R. (2011). Identification of adult midgut precursors in Drosophila. Gene Expr. Patterns 11, 12-21. https://doi.org/10.1016/j.gep.2010.08.005.



- 10. Micchelli, C.A. (2012). The origin of intestinal stem cells in Drosophila. Dev. Dyn. 241, 85-91. https://doi.org/10.1002/dvdy.22759.
- 11. Tepass, U., and Hartenstein, V. (1994). Epithelium formation in the Drosophila midgut depends on the interaction of endoderm and mesoderm. Development 120, 579-590.
- 12. Campbell, K., Whissell, G., Franch-Marro, X., Batlle, E., and Casanova, J. (2011). Specific GATA factors act as conserved inducers of an endodermal-EMT. Dev. Cell 21, 1051-1061. https://doi.org/10.1016/j.devcel.
- 13. Skaer, H. (1993). The alimentary canal. In Developmental Biology of Drosophila melanogaster, M. Bate and A. Martinez-Ariaz, eds., pp. 941-1012.
- 14. Campbell, K., and Casanova, J. (2015). A role for E-cadherin in ensuring cohesive migration of a heterogeneous population of non-epithelial cells. Nat. Commun. 6, 7998. https://doi.org/10.1038/ncomms8998.
- 15. Tepass, U., and Hartenstein, V. (1995). Neurogenic and proneural genes control cell fate specification in the Drosophila endoderm. Development 121, 393-405.
- 16. Campos-Ortega, J.A. (1993). Early neurogenesis in Drosophila melanogaster. In The Development of Drosophila melanogaster, M. Bate and A. Martinez-Ariaz, eds. (Cold Spring Harbor Laboratory Press), pp. 1091-1129.
- 17. Takashima, S., Adams, K.L., Ortiz, P.A., Ying, C.T., Moridzadeh, R., Younossi-Hartenstein, A., and Hartenstein, V. (2011). Development of the Drosophila entero-endocrine lineage and its specification by the Notch signaling pathway. Dev. Biol. 353, 161-172. https://doi.org/10. 1016/j.ydbio.2011.01.039.
- 18. Broadie, K., Skaer, H., and Bate, M. (1992). Whole-embryo culture of Drosophila: development of embryonic tissues in vitro. Rouxs Arch. Dev. Biol. 201, 364-375. https://doi.org/10.1007/BF00365124.
- 19. Trapnell, C., Cacchiarelli, D., Grimsby, J., Pokharel, P., Li, S., Morse, M., Lennon, N.J., Livak, K.J., Mikkelsen, T.S., and Rinn, J.L. (2014). The dynamics and regulators of cell fate decisions are revealed by pseudotemporal ordering of single cells. Nat. Biotechnol. 32, 381-386. https://doi. ora/10.1038/nbt.2859.
- 20. Izumi, Y., Motoishi, M., Furuse, K., and Furuse, M. (2016). A tetraspanin regulates septate junction formation in Drosophila midgut. J. Cell Sci. 129, 1155-1164. https://doi.org/10.1242/jcs.180448.
- 21. Izumi, Y., Yanagihashi, Y., and Furuse, M. (2012). A novel protein complex, Mesh-Ssk, is required for septate junction formation in the Drosophila midgut. J. Cell Sci. 125, 4923-4933. https://doi.org/10.1242/jcs.112243.
- 22. Izumi, Y., Furuse, K., and Furuse, M. (2021). The novel membrane protein Hoka regulates septate junction organization and stem cell homeostasis in the Drosophila gut. J. Cell Sci. 134, jcs257022. https://doi.org/10.1242/ jcs.257022.
- 23. Hernández de Madrid, B., and Casanova, J. (2018). GATA factor genes in the Drosophila midgut embryo. PLoS One 13, e0193612. https://doi.org/ 10.1371/journal.pone.0193612.
- 24. Oliver, G., Sosa-Pineda, B., Geisendorf, S., Spana, E.P., Doe, C.Q., and Gruss, P. (1993). Prox 1, a prospero-related homeobox gene expressed during mouse development. Mech. Dev. 44, 3-16. https://doi.org/10. 1016/0925-4773(93)90012-m.
- 25. Spana, E.P., and Doe, C.Q. (1995). The prospero transcription factor is asymmetrically localized to the cell cortex during neuroblast mitosis in Drosophila. Development 121, 3187-3195. https://doi.org/10.1242/dev.
- 26. Hirata, J., Nakagoshi, H., Nabeshima, Y., and Matsuzaki, F. (1995). Asymmetric segregation of the homeodomain protein Prospero during Drosophila development. Nature 377, 627-630. https://doi.org/10.1038/
- 27. Skafida, E., Delidakis, C., and Monastirioti, M. (2022). Expression of Hey marks a subset of enteroendocrine cells in the Drosophila embryonic and larval midgut. Int. J. Dev. Biol. 66, 223-233. https://doi.org/10.1387/

- 28. Guo, X., Zhang, Y., Huang, H., and Xi, R. (2022). A hierarchical transcription factor cascade regulates enteroendocrine cell diversity and plasticity in Drosophila. Nat. Commun. 13, 6525. https://doi.org/10.1038/s41467-022-34270-0.
- 29. Guo, Z., and Ohlstein, B. (2015). Stem cell regulation. Bidirectional Notch signaling regulates Drosophila intestinal stem cell multipotency. Science 350, aab0988. https://doi.org/10.1126/science.aab0988.
- 30. Wilson, M.M., Weinberg, R.A., Lees, J.A., and Guen, V.J. (2020). Emerging mechanisms by which EMT programs control stemness. Trends Cancer 6, 775-780. https://doi.org/10.1016/j.trecan.2020.03.011.
- 31. Weaver, T.A., and White, R.A. (1995). headcase, an imaginal specific gene required for adult morphogenesis in Drosophila melanogaster. Development 121, 4149-4160. https://doi.org/10.1242/dev.121.12.4149.
- 32. Giannios, P., and Casanova, J. (2021). Systemic and local effect of the Drosophila headcase gene and its role in stress protection of Adult Progenitor Cells. PLoS Genet. 17, e1009362. https://doi.org/10.1371/journal.pgen.1009362.
- 33. Smith, A.V., and Orr-Weaver, T.L. (1991). The regulation of the cell cycle during Drosophila embryogenesis: the transition to polyteny. Development 112, 997-1008. https://doi.org/10.1242/dev.112.4.997.
- 34. Sigrist, S.J., and Lehner, C.F. (1997). Drosophila fizzy-related down-regulates mitotic cyclins and is required for cell proliferation arrest and entry into endocycles. Cell 90, 671-681. https://doi.org/10.1016/s0092-8674(00)80528-0.
- 35. Cohen, E., Allen, S.R., Sawyer, J.K., and Fox, D.T. (2018). Fizzy-Related dictates A cell cycle switch during organ repair and tissue growth responses in the Drosophila hindgut. eLife 7, e38327. https://doi.org/10. 7554/eLife.38327.
- 36. Strand, M., and Micchelli, C.A. (2011). Quiescent gastric stem cells maintain the adult Drosophila stomach. Proc. Natl. Acad. Sci. USA 108, 17696-17701. https://doi.org/10.1073/pnas.1109794108.
- 37. Mehrotra, S., Bansal, P., Oli, N., Pillai, S.J., and Galande, S. (2020). Defective proventriculus regulates cell specification in the gastric region of drosophila intestine. Front. Physiol. 11, 711. https://doi.org/10.3389/ fphys.2020.00711.
- 38. Dubreuil, R.R., Frankel, J., Wang, P., Howrylak, J., Kappil, M., and Grushko, T.A. (1998). Mutations of alpha spectrin and labial block cuprophilic cell differentiation and acid secretion in the middle midgut of Drosophila larvae. Dev. Biol. 194, 1-11. https://doi.org/10.1006/dbio. 1997.8821.
- 39. Filshie, B.K., Poulson, D.F., and Waterhouse, D.F. (1971). Ultrastructure of the copper-accumulating region of the Drosophila larval midgut. Tissue Cell 3, 77-102. https://doi.org/10.1016/s0040-8166(71)80033-2.
- 40. Southall, T.D., and Brand, A.H. (2009). Neural stem cell transcriptional networks highlight genes essential for nervous system development. EMBO J. 28, 3799-3807. https://doi.org/10.1038/emboj.2009.309.
- 41. Chia, W., Somers, W.G., and Wang, H. (2008). Drosophila neuroblast asymmetric divisions: cell cycle regulators, asymmetric protein localization, and tumorigenesis. J. Cell Biol. 180, 267-272. https://doi.org/10. 1083/icb.200708159.
- 42. Kraut, R., and Campos-Ortega, J.A. (1996). inscuteable, a neural precursor gene of Drosophila, encodes a candidate for a cytoskeleton adaptor protein. Dev. Biol. 174, 65-81. https://doi.org/10.1006/dbio.1996.0052.
- 43. Homem, C.C.F., and Knoblich, J.A. (2012). Drosophila neuroblasts: a model for stem cell biology. Development 139, 4297-4310. https://doi. ora/10.1242/dev.080515.
- 44. Shen, C.P., Jan, L.Y., and Jan, Y.N. (1997). Miranda is required for the asymmetric localization of Prospero during mitosis in Drosophila. Cell 90, 449-458. https://doi.org/10.1016/s0092-8674(00)80505-x.
- 45. Ikeshima-Kataoka, H., Skeath, J.B., Nabeshima, Y., Doe, C.Q., and Matsuzaki, F. (1997). Miranda directs Prospero to a daughter cell during Drosophila asymmetric divisions. Nature 390, 625-629. https://doi.org/ 10.1038/37641.

#### **Article**



- Kraut, R., Chia, W., Jan, L.Y., Jan, Y.N., and Knoblich, J.A. (1996). Role of inscuteable in orienting asymmetric cell divisions in Drosophila. Nature 383, 50–55. https://doi.org/10.1038/383050a0.
- Siegrist, S.E., and Doe, C.Q. (2005). Microtubule-induced Pins/Galphai cortical polarity in Drosophila neuroblasts. Cell 123, 1323–1335. https:// doi.org/10.1016/j.cell.2005.09.043.
- Schober, M., Schaefer, M., and Knoblich, J.A. (1999). Bazooka recruits Inscuteable to orient asymmetric cell divisions in Drosophila neuroblasts. Nature 402, 548–551. https://doi.org/10.1038/990135.
- Wodarz, A., Ramrath, A., Kuchinke, U., and Knust, E. (1999). Bazooka provides an apical cue for Inscuteable localization in Drosophila neuroblasts. Nature 402, 544–547. https://doi.org/10.1038/990128.
- Peng, C.Y., Manning, L., Albertson, R., and Doe, C.Q. (2000). The tumoursuppressor genes Igl and dlg regulate basal protein targeting in Drosophila neuroblasts. Nature 408, 596–600. https://doi.org/10.1038/35046094.
- Biteau, B., and Jasper, H. (2014). Slit/Robo signaling regulates cell fate decisions in the intestinal stem cell lineage of Drosophila. Cell Rep. 7, 1867–1875. https://doi.org/10.1016/j.celrep.2014.05.024.
- Wang, C., Guo, X., Dou, K., Chen, H., and Xi, R. (2015). Ttk69 acts as a master repressor of enteroendocrine cell specification in Drosophila intestinal stem cell lineages. Development 142, 3321–3331. https://doi.org/10. 1242/dev.123208.
- Zeng, X., and Hou, S.X. (2015). Enteroendocrine cells are generated from stem cells through a distinct progenitor in the adult Drosophila posterior midgut. Development 142, 644–653. https://doi.org/10.1242/dev.113357.
- Chen, J., Xu, N., Wang, C., Huang, P., Huang, H., Jin, Z., Yu, Z., Cai, T., Jiao, R., and Xi, R. (2018). Transient scute activation via a self-stimulatory loop directs enteroendocrine cell pair specification from self-renewing intestinal stem cells. Nat. Cell Biol. 20, 152–161. https://doi.org/10.1038/ s41556-017-0020-0.
- Choksi, S.P., Southall, T.D., Bossing, T., Edoff, K., de Wit, E., Fischer, B.E., van Steensel, B., Micklem, G., and Brand, A.H. (2006). Prospero acts as a binary switch between self-renewal and differentiation in Drosophila neural stem cells. Dev. Cell 11, 775–789. https://doi.org/10.1016/j.devcel. 2006.09.015
- Karlsson, D., Baumgardt, M., and Thor, S. (2010). Segment-specific neuronal subtype specification by the integration of anteroposterior and temporal cues. PLoS Biol. 8, e1000368. https://doi.org/10.1371/journal. pbio.1000368.
- Kumar, R., Chotaliya, M., Vuppala, S., Auradkar, A., Palasamudrum, K., and Joshi, R. (2015). Role of Homothorax in region specific regulation of Deformed in embryonic neuroblasts. Mech. Dev. 138, 190–197. https:// doi.org/10.1016/j.mod.2015.09.003.
- Rieckhof, G.E., Casares, F., Ryoo, H.D., Abu-Shaar, M., and Mann, R.S. (1997). Nuclear translocation of extradenticle requires homothorax, which encodes an extradenticle-related homeodomain protein. Cell 91, 171–183. https://doi.org/10.1016/s0092-8674(00)80400-6.
- Corsetti, E., and Azpiazu, N. (2013). Functional dissection of the splice variants of the Drosophila gene homothorax (hth). Dev. Biol. 384, 72–82. https://doi.org/10.1016/j.ydbio.2013.09.018.
- Monastirioti, M., Giagtzoglou, N., Koumbanakis, K.A., Zacharioudaki, E., Deligiannaki, M., Wech, I., Almeida, M., Preiss, A., Bray, S., and Delidakis, C. (2010). Drosophila Hey is a target of Notch in asymmetric divisions during embryonic and larval neurogenesis. Development 137, 191–201. https://doi.org/10.1242/dev.043604.
- Wu, S., Yang, Y., Tang, R., Zhang, S., Qin, P., Lin, R., Rafel, N., Lucchetta, E.M., Ohlstein, B., and Guo, Z. (2023). Apical-basal polarity precisely determines intestinal stem cell number by regulating Prospero threshold. Cell Rep. 42, 112093. https://doi.org/10.1016/j.celrep.2023.112093.
- 62. Buescher, M., Yeo, S.L., Udolph, G., Zavortink, M., Yang, X., Tear, G., and Chia, W. (1998). Binary sibling neuronal cell fate decisions in the Drosophila embryonic central nervous system are nonstochastic and require inscuteable-mediated asymmetry of ganglion mother cells. Genes Dev. 12, 1858–1870. https://doi.org/10.1101/gad.12.12.1858.

- Beehler-Evans, R., and Micchelli, C.A. (2015). Generation of enteroendocrine cell diversity in midgut stem cell lineages. Development 142, 654–664. https://doi.org/10.1242/dev.114959.
- 64. Guo, X., Yin, C., Yang, F., Zhang, Y., Huang, H., Wang, J., Deng, B., Cai, T., Rao, Y., and Xi, R. (2019). The cellular diversity and transcription factor code of drosophila enteroendocrine cells. Cell Rep. 29, 4172–4185.e5. https://doi.org/10.1016/j.celrep.2019.11.048.
- Lehmann, R. (2012). Germline stem cells: origin and destiny. Cell Stem Cell 10, 729–739. https://doi.org/10.1016/j.stem.2012.05.016.
- Yoshiura, S., Ohta, N., and Matsuzaki, F. (2012). Tre1 GPCR signaling orients stem cell divisions in the Drosophila central nervous system. Dev. Cell 22, 79–91. https://doi.org/10.1016/j.devcel.2011.10.027.
- Pitsidianaki, I., Morgan, J., Adams, J., and Campbell, K. (2021).
   Mesenchymal-to-epithelial transitions require tissue-specific interactions with distinct laminins. J. Cell Biol. 220, e202010154. https://doi.org/10.1083/jcb.202010154.
- Simões, S., Oh, Y., Wang, M.F.Z., Fernandez-Gonzalez, R., and Tepass, U. (2017). Myosin II promotes the anisotropic loss of the apical domain during Drosophila neuroblast ingression. J. Cell Biol. 216, 1387–1404. https://doi.org/10.1083/jcb.201608038.
- Eisenhoffer, G.T., Loftus, P.D., Yoshigi, M., Otsuna, H., Chien, C.B., Morcos, P.A., and Rosenblatt, J. (2012). Crowding induces live cell extrusion to maintain homeostatic cell numbers in epithelia. Nature 484, 546–549. https://doi.org/10.1038/nature10999.
- Rosenblatt, J., Raff, M.C., and Cramer, L.P. (2001). An epithelial cell destined for apoptosis signals its neighbors to extrude it by an actinand myosin-dependent mechanism. Curr. Biol. 11, 1847–1857. https:// doi.org/10.1016/s0960-9822(01)00587-5.
- Zhang, S., Wu, S., Yao, R., Wei, X., Ohlstein, B., and Guo, Z. (2024).
   Eclosion muscles secrete ecdysteroids to initiate asymmetric intestinal stem cell division in Drosophila. Dev. Cell 59, 125–140.e12. https://doi. org/10.1016/j.devcel.2023.11.016.
- Brand, A.H., and Livesey, F.J. (2011). Neural stem cell biology in vertebrates and invertebrates: more alike than different? Neuron 70, 719–729. https://doi.org/10.1016/j.neuron.2011.05.016.
- Musser, J.M., Schippers, K.J., Nickel, M., Mizzon, G., Kohn, A.B., Pape, C., Ronchi, P., Papadopoulos, N., Tarashansky, A.J., Hammel, J.U., et al. (2021). Profiling cellular diversity in sponges informs animal cell type and nervous system evolution. Science 374, 717–723. https://doi. org/10.1126/science.abj2949.
- Steinmetz, P.R.H., Aman, A., Kraus, J.E.M., and Technau, U. (2017). Gut-like ectodermal tissue in a sea anemone challenges germ layer homology.
   Nat. Ecol. Evol. 1, 1535–1542. https://doi.org/10.1038/s41559-017-0285-5.
- Steger, J., Cole, A.G., Denner, A., Lebedeva, T., Genikhovich, G., Ries, A., Reischl, R., Taudes, E., Lassnig, M., and Technau, U. (2022). Single-cell transcriptomics identifies conserved regulators of neuroglandular lineages. Cell Rep. 40, 111370. https://doi.org/10.1016/j.celrep.2022.111370.
- Tournière, O., Gahan, J.M., Busengdal, H., Bartsch, N., and Rentzsch, F. (2022). Insm1-expressing neurons and secretory cells develop from a common pool of progenitors in the sea anemone Nematostella vectensis. Sci. Adv. 8, eabi7109. https://doi.org/10.1126/sciadv.abi7109.
- Bhalerao, S., Berdnik, D., Török, T., and Knoblich, J.A. (2005).
   Localization-dependent and -independent roles of numb contribute to cell-fate specification in Drosophila. Curr. Biol. 15, 1583–1590. https://doi.org/10.1016/j.cub.2005.07.061.
- Ramat, A., Hannaford, M., and Januschke, J. (2017). Maintenance of Miranda localization in drosophila neuroblasts involves interaction with the cognate mRNA. Curr. Biol. 27, 2101–2111.e5. https://doi.org/10. 1016/j.cub.2017.06.016.
- Couturier, L., Mazouni, K., and Schweisguth, F. (2013). Numb localizes at endosomes and controls the endosomal sorting of notch after asymmetric division in Drosophila. Curr. Biol. 23, 588–593. https://doi.org/10.1016/j. cub.2013.03.002



- 80. Gomez, J.M., Chumakova, L., Bulgakova, N.A., and Brown, N.H. (2016). Microtubule organization is determined by the shape of epithelial cells. Nat. Commun. 7, 13172. https://doi.org/10.1038/ncomms13172.
- 81. Weng, M., and Wieschaus, E. (2016). Myosin-dependent remodeling of adherens junctions protects junctions from Snail-dependent disassembly. J. Cell Biol. 212, 219-229. https://doi.org/10.1083/jcb.201508056.
- 82. Yanagihashi, Y., Usui, T., Izumi, Y., Yonemura, S., Sumida, M., Tsukita, S., Uemura, T., and Furuse, M. (2012). Snakeskin, a membrane protein associated with smooth septate junctions, is required for intestinal barrier function in Drosophila. J. Cell Sci. 125, 1980-1990. https://doi.org/10.1242/
- 83. Garces, A., and Thor, S. (2006). Specification of Drosophila aCC motoneuron identity by a genetic cascade involving even-skipped, grain and zfh1. Development 133, 1445-1455. https://doi.org/10.1242/dev.02321.
- 84. Lee, C.Y., Wilkinson, B.D., Siegrist, S.E., Wharton, R.P., and Doe, C.Q. (2006). Brat is a Miranda cargo protein that promotes neuronal differentiation and inhibits neuroblast self-renewal. Dev. Cell 10, 441-449. https:// doi.org/10.1016/j.devcel.2006.01.017.
- 85. Kurant, E., Pai, C.Y., Sharf, R., Halachmi, N., Sun, Y.H., and Salzberg, A. (1998). Dorsotonals/homothorax, the Drosophila homologue of meis1, interacts with extradenticle in patterning of the embryonic PNS. Development 125, 1037-1048. https://doi.org/10.1242/dev.125.6.1037.
- 86. Konstantinides, N., Holguera, I., Rossi, A.M., Escobar, A., Dudragne, L., Chen, Y.C., Tran, T.N., Martínez Jaimes, A.M., Özel, M.N., Simon, F., et al. (2022). A complete temporal transcription factor series in the fly visual system. Nature 604, 316-322. https://doi.org/10.1038/s41586-022-04564-w.
- 87. Choi, H.M.T., Calvert, C.R., Husain, N., Huss, D., Barsi, J.C., Deverman, B.E., Hunter, R.C., Kato, M., Lee, S.M., Abelin, A.C.T., et al. (2016). Mapping a multiplexed zoo of mRNA expression. Development 143, 3632-3637. https://doi.org/10.1242/dev.140137.

- 88. Choi, H.M.T., Schwarzkopf, M., Fornace, M.E., Acharya, A., Artavanis, G., Stegmaier, J., Cunha, A., and Pierce, N.A. (2018). Third-generation in situ hybridization chain reaction: multiplexed, quantitative, sensitive, versatile, robust. Development 145, dev165753. https://doi.org/10.1242/dev. 165753.
- 89. R Core Team (2021). R: A Language and Environment for Statistical Computing (R Foundation for Statistical Computing).
- 90. Hao, Y., Hao, S., Andersen-Nissen, E., Mauck, W.M., 3rd, Zheng, S., Butler, A., Lee, M.J., Wilk, A.J., Darby, C., Zager, M., et al. (2021). Integrated analysis of multimodal single-cell data. Cell 184, 3573-3587.e29. https://doi.org/10.1016/j.cell.2021.04.048.
- 91. van Dijk, D., Sharma, R., Nainys, J., Yim, K., Kathail, P., Carr, A.J., Burdziak, C., Moon, K.R., Chaffer, C.L., Pattabiraman, D., et al. (2018). Recovering gene interactions from single-cell data using data diffusion. Cell 174, 716-729.e27. https://doi.org/10.1016/j.cell.2018.05.061.
- 92. Carlson, M. (2019). org.Dm.eg.db: Genome wide annotation for Fly. R package version 3.8.2.
- 93. Liberzon, A., Birger, C., Thorvaldsdóttir, H., Ghandi, M., Mesirov, J.P., and Tamayo, P. (2015). The Molecular Signatures Database (MSigDB) hallmark gene set collection. Cell Syst. 1, 417-425. https://doi.org/10.1016/j.cels. 2015.12.004.
- 94. Durinck, S., Spellman, P.T., Birney, E., and Huber, W. (2009). Mapping identifiers for the integration of genomic datasets with the R/Bioconductor package biomaRt. Nat. Protoc. 4, 1184-1191. https:// doi.org/10.1038/nprot.2009.97.
- 95. Bienz, M. (1997). Endoderm induction in Drosophila: the nuclear targets of the inducing signals. Curr. Opin. Genet. Dev. 7, 683-688. https://doi.org/ 10.1016/s0959-437x(97)80017-2.



#### **STAR**\***METHODS**

#### **KEY RESOURCES TABLE**

REAGENT or RESOURCE	SOURCE	IDENTIFIER
Antibodies		
Goat anti-GFP	Abcam	Cat#: AB6673; RRID: AB_305643
Rabbit anti-GFP	Chromotek	Cat#: PABG1; RRID: AB_2749857
Mouse anti-Prospero	Developmental Studies Hybridoma Bank (DSHB)	RRID: AB_528440
Rabbit anti-Snakeskin	Yanagihashi et al. <sup>82</sup>	RRID: AB_2570187
Guinea pig anti-Snail	Weng and Wieschaus <sup>81</sup>	N/A
Mouse anti-Hindsight	Developmental Studies Hybridoma Bank (DSHB)	RRID: AB_528278
Rat anti-Grain	Garces and Thor <sup>83</sup>	RRID: AB_2567715
Rabbit anti-Bazooka	Wodarz et al. <sup>49</sup>	N/A
Rabbit anti-aPKC	Santa Cruz Biotechnology	Cat#: sc-216; RRID: AB_2300359
Mouse anti-alpha Tubulin	Sigma-Aldrich	Cat#: T6199; RRID: AB_477583
Guinea pig anti-Miranda	Ramat et al. <sup>78</sup>	N/A
Guinea pig anti-Forkhead	Gift from Jordi Casanova (IRB Barcelona)	N/A
Rat anti-Brat	Lee et al. <sup>84</sup>	N/A
Rabbit anti-Homothorax	Kurant et al. <sup>85</sup>	RRID: AB_2568819
Rat anti-Escargot	Konstantinides et al.86	N/A
Guinea pig anti-Hey	Monastirioti et al. <sup>60</sup>	RRID: AB_2568888
Donkey anti-Goat Alexa Fluor Plus 488	Thermo Fisher Scientific	Cat#: A32814; RRID: AB_2762838
Donkey anti-Rabbit Alexa Fluor Plus 488	Thermo Fisher Scientific	Cat#: A32790; RRID: AB_2866495
Donkey anti-Mouse Alexa Fluor Plus 555	Thermo Fisher Scientific	Cat#: A32773; RRID: AB_2762848
Donkey anti-Rat Alexa Fluor Plus 555	Thermo Fisher Scientific	Cat#: A48270; RRID: AB_2896336
Donkey anti-Rabbit Alexa Fluor Plus 555	Thermo Fisher Scientific	Cat#: A32794; RRID: AB_2762834
Donkey anti-Mouse Alexa Fluor Plus 647	Thermo Fisher Scientific	Cat#: A32787; RRID: AB_2762830
Goat anti-Guinea pig Alexa Fluor 647	Thermo Fisher Scientific	Cat#: A-21450; RRID: AB_2535867
Donkey anti-Guinea pig Cy5	Jackson ImmunoResearch	RRID: AB_2340462
Chemicals, peptides, and recombinant proteins		
DAPI	Sigma-Aldrich	Cat#: D9542-10mg; CAS#: 28718-90-3
ProLong Glass Antifade Mountant	Thermo Fisher Scientific	Cat#: P36980
Formaldehyde solution	Sigma-Aldrich	Cat#: F8775-25ml; CAS#: 50-00-0
Ultra-pure methanol-free formaldehyde solution	Polysciences	Cat#: 18814-10; CAS#: 50-00-0
Bovine Serum Albumin Fraction V	Roche	Cat#: 10735078001
Phosphate Buffered Saline	Corning	Cat#: 21-040-CM
AccuGENE 20x Saline Sodium Citrate (SSC) Buffer	Lonza	Cat#: 51205
Glycerol	VWR	Cat#: 84730.0001; CAS#: 56-81-5
Friton X-100	Bio-Rad	Cat#: 1610407; CAS#: 9002-93-1
Probe Hybridisation Buffer	Molecular Instruments	N/A
Probe Wash Buffer	Molecular Instruments	N/A
Amplification Buffer	Molecular Instruments	N/A
Poly-L-Lysine	Sigma-Aldrich	Cat#: P4707-50ml; CAS#: 25998-63-0
Methanol	Fisher Scientific	Cat#: 10675112; CAS#: 67-56-1
Heptane	Honeywell	Cat#: H2198; CAS#: 142-82-5
TrypLE Express	Gibco	Cat#: 12604013
10% Bovine Serum Albumin in PBS, pH 7.4, sterile	Bioworld	Cat#: 21420068-1

(Continued on next page)



SOURCE	
SOUNCE	IDENTIFIER
Thermo Fisher Scientific	Cat#: EO0381
10x Genomics	PN-1000075
10x Genomics	Cat#: 2000060
Thermo Fisher Scientific	Cat#: 37002D
Beckman Coulter	Cat#: 15676104
Agilent	Cat#: 5067-4626
Kapa	Cat#: 07960417001
Sigma-Aldrich	Cat#: S5881-500G
Illumina	Cat#: FC-110-3001
Applied Biosystems	Cat#: 4309155
Thermo Fisher Scientific	Cat#: Q32851
This paper	Biostudies: E-MTAB-13247
Carlson <sup>92</sup>	https://bioconductor.org/packages/
	release/data/annotation/html/
	org.Dm.eg.db.html
Liberzon et al. <sup>93</sup>	https://www.gsea-msigdb.org/ gsea/msigdb
Global Core Biodata Resource	http://geneontology.org/docs/ download-ontology/
Bloomington Drosophila Stock Center	BDSC: 5; Flybase: FBsn0000277
Gift from Helen Skaer (University of Cambridge)	N/A
Bloomington Drosophila Stock Center	BDSC: 4935; Flybase: FBal0063393
Bloomington Drosophila Stock Center	BDSC: 84277, Flybase: FBti0074589
Ramat et al. <sup>78</sup>	Flybase: FBal0361103
Couturier et al. <sup>79</sup>	Flybase: FBal0300974
Bloomington Drosophila Stock Center	BDSC: 66463; Flybase: FBal0280034
Bloomington Drosophila Stock Center	BDSC: 59793; Flybase: FBti0178502
Bloomington Drosophila Stock Center	BDSC: 68183; Flybase: FBti0187379
Bloomington Drosophila Stock Center	BDSC: 80572; Flybase: FBti0201782
Bloomington Drosophila Stock Center	BDSC: 66670; Flybase: FBal0082443
Bloomington Drosophila Stock Center	BDSC: 5458; Flybase: FBal0032479
Bloomington Drosophila Stock Center	BDSC: 39678; Flybase: FBal0046159
Bloomington Drosophila Stock Center	BDSC: 36283; Flybase: FBal0002683
Bloomington Drosophila Stock Center	BDSC: 7637; Flybase: FBab0038213
Bloomington Drosophila Stock Center	BDSC: 4096; Flybase: FBti0002470
Molecular Instruments	N/A
Molecular Instruments	N/A
Molecular Instruments	Accession Number: NM_167625.3
	_
Molecular Instruments	Accession Number: NM 1676253
Molecular Instruments  Molecular Instruments	Accession Number: NM_167625.3  Accession Number: NM_001260116.2
Molecular Instruments	Accession Number: NM_001260116.2
Molecular Instruments Molecular Instruments	Accession Number: NM_001260116.2 Accession Number: NM_057384.4
Molecular Instruments Molecular Instruments Molecular Instruments	Accession Number: NM_001260116.2 Accession Number: NM_057384.4 Accession Number: NM_079323.4
Molecular Instruments Molecular Instruments	Accession Number: NM_001260116.2 Accession Number: NM_057384.4
	Thermo Fisher Scientific Beckman Coulter Agilent Kapa Sigma-Aldrich Illumina Applied Biosystems Thermo Fisher Scientific  This paper Carlson <sup>92</sup> Liberzon et al. <sup>93</sup> Global Core Biodata Resource  Bloomington Drosophila Stock Center Gift from Helen Skaer (University of Cambridge) Bloomington Drosophila Stock Center Bloomington Drosophila Stock Center Ramat et al. <sup>78</sup> Couturier et al. <sup>79</sup> Bloomington Drosophila Stock Center

(Continued on next page)

#### **Article**



Continued		
REAGENT or RESOURCE	SOURCE	IDENTIFIER
B2 546 HCR amplifier	Molecular Instruments	N/A
B2 647 HCR amplifier	Molecular Instruments	N/A
B3 488 HCR amplifier	Molecular Instruments	N/A
B4 488 HCR amplifier	Molecular Instruments	N/A
B4 647 HCR amplifier	Molecular Instruments	N/A
Software and algorithms		
Fiji	Fiji	https://imagej.net/Fiji/Downloads
Zen Blue v2.3	Carl Zeiss Inc.	N/A
Zen Black v2.3	Carl Zeiss Inc.	N/A
Cellranger v4-0.0 and v3.0.2	10x Genomics	https://www.10xgenomics.com/ support/software/cell-ranger/latest
R	The R Foundation	https://www.r-project.org/
Seurat v4.1.1	Hao et al. 90	https://satijalab.org/seurat/; RRID: SCR_016341
RMagic (v2.0.3)	van Dijk et al. <sup>91</sup>	https://github.com/cran/Rmagic
Monocle v3_1.0.0	Trapnell et al. <sup>19</sup>	http://cole-trapnell-lab.github.io/monocle-release/

#### **EXPERIMENTAL MODEL AND STUDY PARTICIPANT DETAILS**

#### Fly Husbandry

Flies were raised at 18°C to 25°C on standard cornmeal food during stock maintenance. During embryo collections, flies were fed on apple juice plates supplemented with yeast paste.

#### Fly strains

Embryos driving UAS-stingerGFP (BDSC 84277) in the midgut using either hkb-Gal4 (a gift from Helen Skaer) or 48Y-Gal4 (BDSC 4935), or OreR (BDSC 5), were used as wildtype controls. Embryos collected for analysis were of mixed sex, with the exception of *dlg1*<sup>14</sup> mutants, which were hemizygous mutant males.

Null mutant alleles used in this study are  $pros^{17}$  (BDSC 5458),  $insc^{22}$  (BDSC 39678), and  $dlg1^{14}$  (BDSC 36283). Df(3R)Exel6158 (BDSC 7637) is a deficiency which abolishes transcription of all hth splice variants except the G isform, the product of which remains cytoplasmic. For reducing the activity of Numb, the hypomorphic  $numb^1$  allele was used (BDSC 4096). All mutant embryos were zygotic mutants but not maternal. Fluorescently tagged stocks used are Mira eGFP, Numb GFP, Pros GFP. FPTB (BDSC 66463), Brat-GFP (59793) and Mirr GFP (BDSC 68183). Lineage tracing in the embryo was performed using Pros-Gal4 (BDSC 80572)

#### **METHOD DETAILS**

#### Drosophila embryo fixation and immunofluorescence

Embryos for standard stainings were dechorionated using 50% bleach for 3 minutes, fixed in 4% PFA for 20 minutes, and then devitellinised with manual shaking. Embryos were permeabilised and blocked in PBS + 0.2% Triton X-100 (PBT) + 0.1% BSA for 2 hours. Primary antibodies were incubated overnight at 4°C, while secondary antibodies were incubated for 2 hours at room temperature. Embryos for microtubule stainings were fixed in accordance with previous studies, 80 and blocked in PBT + 5% BSA for 2 hours. Primary antibodies used were: goat anti-GFP 1:500 (AB6673), rabbit anti-GFP 1:1000 (PABG1), mouse anti-prospero 1:100 (MR1A), guinea pig anti-Snail 1:1000<sup>81</sup> (a gift from Mo Weng), mouse anti-Hindsight 1:20 (1G9), rabbit anti-Snakeskin 1:200<sup>82</sup> (a gift from Mikio Furuse), rat anti-Grain 1:200 (Ab87)83 (a gift from Alain Garces), rabbit anti-Bazooka N-term 1:20049 (a gift from Andreas Wodarz), rabbit anti-aPKC 1:200 (sc-216), mouse anti-αTubulin 1:200 (T6199), guinea pig anti-Miranda 1:400<sup>78</sup> (a gift from Jens Januschke), guinea pig anti-Forkhead 1:500 (a gift from Jordi Casanova), rat anti-brat84 1:100 (a gift from Robin Wharton), rabbit anti-Homothorax<sup>85</sup> (a gift from Barry Denholm), rat anti-Escargot<sup>86</sup> 1:200 (a gift from Claude Desplan) and guinea pig anti-Hey 1:1000<sup>60</sup> (a gift from Maria Monastirioti). DAPI was used as a DNA stain at a concentration of 1:250. Secondary antibodies, used at a concentration ranging from 1:100-200, were as follows: Donkey anti-Goat Alexa Fluor Plus 488 (A32814), Donkey anti-Rabbit Alexa Fluor Plus 488 (A32790), Donkey anti-Mouse Alexa Fluor Plus 555 (A32773), Donkey anti-Rat Alexa Fluor Plus 555 (A48270), Donkey anti-Rabbit Alexa Fluor Plus 555 (A32794), Donkey anti-Mouse Alexa Fluor Plus 647 (A32787), Goat anti-Guinea Pig Alexa Fluor 647 (A-21450), and Donkey anti-Guinea Pig Cy5 (Jackson ImmunoResearch; AB\_2340462). Unless otherwise stated, secondary antibodies were sourced from Thermo Fisher Scientific. Embryos were mounted in ProLong Glass Antifade Mountant (Thermo Scientific).



#### HCR in situ hybridisation

HCR *in situ* hybridisation was performed using an adapted versions of previously-published protocols. HCR v3.0 probes (*d2eGFP*-B3, *eGFP*-B3, *Bx*-B1, *Bx*-B2, *pros*-B1, *sna*-B4, *hth*-B2 and *mirr*-B2) and hairpins (B1 546, B1 647, B2 546, B2 647, B3 488, B4 488 and B4 647) were synthesised by Molecular Instruments. Following standard fixation, embryos were incubated in Probe Hybridization Buffer (Molecular Instruments) at 37°C for 30 minutes then hybridised with Probe Hybridisation Buffer (Molecular Instruments) containing HCR probes overnight at 37°C. Embryos were washed four times for 15 minutes each, using pre-warmed Probe Wash Buffer (Molecular Instruments) at 37°C. Embryos were then washed twice at room temperature in 5x SSC buffer, pre-amplified in Probe Amplification Buffer (Molecular Instruments) for 10 minutes, and then incubated overnight in Probe Amplification Buffer containing snap-cooled HCR hairpins at room temperature in the dark. Excess hairpins were removed with two 5 min washes with 5x SSC, followed by 2 washes for 30 minutes and a final 5 minute wash in 5x SSC. Embryos were mounted in ProLong Glass Antifade Mountant (Thermo Scientific).

#### **Image collection**

Confocal images were generated using a Zeiss LSM880 with the Plan-Apochromat 25x/0.8 multi-immersion lens with oil, Plan-Apochromat 40x/1.3 oil immersion lens, or the Plan-Apochromat 63x/1.4 oil-immersion lens. Images were captured with either the internal GaAsP detector or an Airyscan detector; Airyscan processing was performed on Zen software. All images in the paper are oriented with the anterior facing the left. Image analysis (detailed below) was performed using Fiji and associated plugins.

#### ScRNAseq methods

#### Sample collection

Living embryos were collected within 2 hour time windows (3.5-5.5 hours (T1) 5-7 hours (T2) 6.5-8.5 (T3) 8-10 hours (T4)). They were dechorionated and gently stuck down on a thin strip of double-sided sticky tape, and the tape mounted on poly-L-lysine coated coverslips. They were covered in cold 0.01% PBS-BSA and dissected by mouth pipetting using sharpened pulled capillary needles as described in. Immediately after dissecting 10 embryos within a 30 mins period, the tissue was pooled and dissociated into single cells by mouth pipetting using pulled glass capillaries while the samples are incubating in 1X of the mild cell dissociation buffer TrypLE Express (Gibco). After a total of 10 mins of time dissociating, cells were fixed in pre-chilled to -20°C Methanol to a final concentration of 80:20 Methanol:PBS and stored at -80°C. Prior to library preparation, 15 samples of 10 embryos were pooled per collection window. Cells were rehydrated in 0.01% PBS-BSA with the RNAase inhibitor RiboLock and filtered through a 20μm cell strainer before resuspending, ready for scRNA library preparation.

#### **Library Generation**

Single cell RNA libraries were generated from each of the four single cell suspensions using the 10x Genomics Chromium single cell 3' reagents kit v3. Cells were mixed with reagents for Gel Beads-in-emulsion (GEM) formation and loaded onto a Chromium Next GEM Chip B for GEM creation. 100µl of each sample was recovered from the chip and placed into tubes and incubated in a GEM reverse transcriptase reaction for 45 mins at 53°C and 5 mins at 85°C. Recovery reagent was added to each sample and the aqueous phase recovered. This was then cleaned with magnetic Dynabeads MyOne silane beads by incubation with the beads at room temperature for 10 mins, 80% ethanol washing of captured beads and finally eluting the sample from the beads. cDNA primers and amplification mix was added and 11 cycles of RT amplification performed. The product was purified with SPRIselect reagent and the recovered sample checked for concentration and profile on an Agilent Bioanalyser high sensitivity chip.

25% of this product was used for library generation. Reagents for fragmentation/end repair were added and the samples heated at 32°C for 5 mins followed by incubation at 65°C for 30 mins. The samples were purified using SPRIselect using a double size selection approach. Adaptor oligos were added by ligation and after a further clean up step, sample indexes (chromium i7 plate single index) were added via 11/12 cycles of PCR, with 12 cycles for samples that had a lower cell count. The final product was cleaned with SPRIselect reagent using a double size selection approach.

#### **Library Sequencing**

The libraries were checked using Qubit assay and the size by an Agilent Bioanalyser high sensitivity chip. Libraries were pooled at an equimolar proportion based on this information and the quantity and quality of the pool was assessed by Qubit and the Bioanalyzer, and subsequently by qPCR using the Illumina Library Quantification Kit from Kapa on a Roche Light Cycler LC480II according to manufacturer's instructions.

For the above qPCR, a 10 µl PCR reaction (performed in triplicate for each pooled library) was prepared on ice with 6 µl SYBR Green I Master Mix and 2 µl diluted pooled DNA (1:1000 to 1:100,000 depending on the initial concentration determined by the Qubit dsDNA HS Assay Kit). PCR thermal cycling conditions consisted of initial denaturation at 95°C for 5 minutes, 35 cycles of 95°C for 30 seconds (denaturation) and 60°C for 45 seconds (annealing and extension), melt curve analysis to 95°C (continuous) and cooling at 37°C (LightCycler LC48011, Roche Diagnostics Ltd, Burgess Hill, UK).

Following calculation of the molarity using qPCR data, template DNA was diluted to 250pM and denatured for 8 mins at room temperature using freshly diluted 0.2 N sodium hydroxide (NaOH) and the reaction was subsequently terminated by the addition of 400mM pH 8 Tris-HCl. To improve sequencing quality control 1% PhiX (Illumina) was spiked in. The libraries were sequenced on the Illumina NovaSeq 6000 platform (Illumina) following the XP workflow on 2 lanes of an SP flow cell at the configuration 28/8/91 as specified by 10x genomics. scRNAseq libraries were sequenced obtaining a total of 1723M raw reads.

#### **Article**



#### ScRNAseq data processing Alignment and read count

Fastq files were processed with the 10x Genomics software Cellranger (v4-0.0) using the *Drosophila melanogaster* reference transcriptome built with genome version r6.32 for data from collection windows (CWs) 1 and 2. For CWs 3 and 4, Cellranger (v3.0.2) and reference 6.29 was used. Default values were used for all parameters. The number of genes and cells detected per sample were: CW1, 23932 genes, 10093 cells; CW2, 23932 genes, 8509 cells; CW3, 17562 genes, 7731 cells; CW4, 17562 genes, 6080 cells.

#### **Normalization**

Count matrices were read into R (v4.1.3)<sup>89</sup> and merged into a single Seurat (v4.1.1) object.<sup>90</sup> All following functions belong to the Seurat package unless specified. Ribosomal genes were excluded from the count matrix and cells with less than 2500 read counts were discarded. After applying quality filters, this resulted in the gene expression profiles of 21796 cells, with an average of 10886 counts and 3919 genes detected per cell. Cell cycle phase scores were computed using the function *CellCycleScoring* with the homologs of the human gene sets included in the Seurat package. Expression was normalized with the *SCT\_transform* function, regressing out the S and G2M scores and the percent of mitochondrial reads per cell.

#### Normalization of the Midgut compartment

We selected cells in the connected component containing Midgut and Malpighian tubules and normalized them following the same procedure as in the whole dataset. To generate two-dimensional maps of midgut cells only, we recalculated the Uniform Manifold Approximation and Projection (UMAP) representation after removing all Malpighian tubule cells. Midgut-only UMAPs were vertically reflected for ease of annotation.

#### Dimensionality reduction and clustering

Dimensionality reduction was performed through the function *RunPCA*, followed by the calculation of the UMAP using the first 12 principal components. Unsupervised clustering was found with the functions *FindNeighbors*, with 12 components, and *FindClusters* with resolution 1.2.

#### Gene expression imputation and smoothing and marker identification

Gene expression was imputed and smoothed using MAGIC (Rmagic v2.0.3). For the Midgut compartment we used 9 principal components for finding clusters. MAGIC expression scores were used for all expression plots. Population markers were found using the function *FindMarkers* with default parameters. Gene set scores were computed as the mean of the Magic expression of the corresponding genes.

#### Annotation of cell populations

Differential expression of unsupervised clusters against the rest of the cells were found and compared to markers of known populations.

#### **Pseudotime computation**

Monocle (v 3\_1.0.0)<sup>19</sup> was used to compute pseudotimes. For the whole dataset the number of centres for the *learn\_graph* function was set to the default value (300 for the midgut subset).

#### Gene set enrichment analysis

Functional enrichment was computed using a hypergeometric test as implemented in the function *phyper* from R. The universe was defined as all the genes in the expression matrix. Gene ontology definitions were downloaded org.DM.eg.db v3.0.0.<sup>92</sup> Broad Hallmarks were downloaded from the Molecular Signatures database v5.1<sup>93</sup> and converted to *Drosophila melanogaster* gene symbols using the biomaRt T package.<sup>94</sup> GOSLIM gene sets were downloaded from http://geneontology.org/docs/download-ontology/ and filtered to retain only main terms.

#### **QUANTIFICATION AND STATISTICAL ANALYSIS**

#### **Cell counting**

Embryos were imaged at stage 15 when intending to count EEs, EE subpopulations, or AMPs. Stage 12 embryos were imaged for ICP cell counts, as this allowed us to count cells in the posterior midgut cluster prior to both its fusion with the anterior midgut and the initiation of signalling from the mesoderm to specify the gastric region. <sup>95</sup> All cells were counted using the Cell Counter plugin. Any Sna<sup>+</sup>Pros<sup>+</sup> cells were considered EEs for the purposes of cell counting.

#### **Spindle orientation**

To quantify spindle orientation, a segmented line was drawn following the apical surface of the midgut epithelium on either side of the endoblast. A third line was drawn to span the endoblast and connect the two lines on either side. A fourth line was drawn along the angle of the mitotic spindle, and the angle of intersection between the third and fourth lines was determined. Mitotic spindle orientation quantification was performed on dividing endoblasts from early stage 10 embryos when endoblasts sit atop the apical layer of the midgut epithelium. During late stage 10 and early stage 11, endoblasts continue dividing concurrent with the epithelial-mesenchymal transition, making orientation of the spindle with respect to the epithelial layer difficult to calculate accurately.



#### Nuclear area and cell size measurement

Nuclear area was calculated by drawing around the border of DAPI signal at the largest z-frame of a nucleus. The Fiji measure tool was then used to determine the area at this widest point. To normalise nuclear size values between embryos, mesoderm nuclei were measured in each embryo and a size value relative to mesoderm nuclei was calculated for each of the midgut AMP and ICP nuclei. Daughter cell sizes during endoblast cell division were measured during anaphase or telophase. A line was drawn between the narrowest points of the cleavage furrow, separating a dividing cell into two daughters. A line was then drawn around the cell cortex for each daughter and the area determined using the measure tool.

#### Neuroblast and endoblast polarity quantification

The Fiji line tool was used to draw a 50 pixel-wide line across the length of a dividing cell, and fluorescence intensity measured. Fluorescence levels were normalised to the maximum intensity value, and normalised for cell length. The line was oriented along the axis of division by drawing the line through the mitotic spindle or, where the mitotic spindle was not stained, drawing the line perpendicular to the DAPI signal at metaphase. To quantify asymmetric segregation of cell fate determinants in wild type versus mutant genotypes, the highest intensity signal in the first 10% versus the last 10% of each cell was used to calculate the proportion of signal segregated along the axis of division.